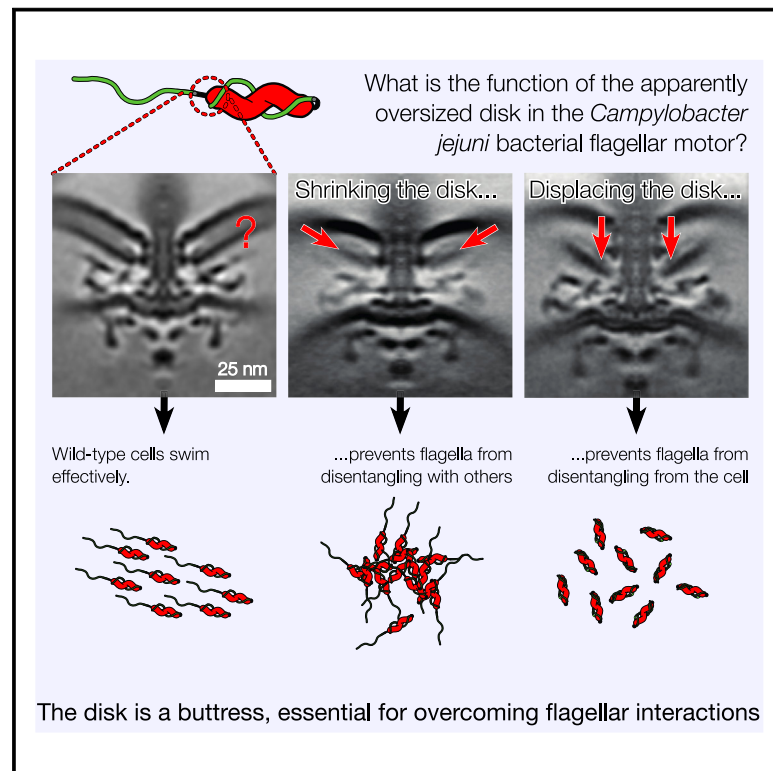


Developmental Cell

Evolution of a large periplasmic disk in *Campylobacterota* flagella enables both efficient motility and autoagglutination

Graphical abstract



Authors

Eli J. Cohen, Tina Drobnič, Deborah A. Ribardo, ..., Daisuke Nakane, David R. Hendrixson, Morgan Beeby

Correspondence

eli.cohen@imperial.ac.uk

In brief

The human pathogen *Campylobacter jejuni* (*C. jejuni*) has a larger, more complex flagellar motor than that of the model organism *Salmonella typhimurium*. In Cohen and Drobnič et al. the authors demonstrate that one function of the added complexity of the motor is to promote efficient directional switching while swimming and to prevent cell clumping.

Highlights

- The *C. jejuni* flagellar motor has an extra-large basal disk
- The basal disk promotes filament unwrapping from the cell surface
- Reduction of cell-surface glycosylation is required for swimming without a basal disk



Article

Evolution of a large periplasmic disk in *Campylobacterota* flagella enables both efficient motility and autoagglutination

Eli J. Cohen,^{1,6,7,*} Tina Drobnic,^{1,6} Deborah A. Ribardo,² Aoba Yoshioka,³ Trishant Umrekar,¹ Xuefei Guo,¹ Jose-Jesus Fernandez,⁴ Emma E. Brock,⁵ Laurence Wilson,⁵ Daisuke Nakane,³ David R. Hendrixson,² and Morgan Beeby¹

¹Department of Life Sciences, Imperial College London, London SW7 2AZ, UK

²Department of Microbiology, University of Texas Southwestern Medical Center, Dallas, TX 75390, USA

³Department of Engineering Science, Graduate School of Informatics and Engineering, The University of Electro-Communications, Tokyo, Japan

⁴Spanish National Research Council (CINN-CSIC), Health Research Institute of Asturias (ISPA), Av Hospital Universitario s/n, Oviedo 33011, Spain

⁵Department of Physics, School of Physics, Engineering and Technology, University of York, York YO10 5DD, UK

⁶These authors contributed equally

⁷Lead contact

*Correspondence: eli.cohen@imperial.ac.uk

<https://doi.org/10.1016/j.devcel.2024.09.008>

SUMMARY

The flagellar motors of *Campylobacter jejuni* (*C. jejuni*) and related *Campylobacterota* (previously epsilonproteobacteria) feature 100-nm-wide periplasmic “basal disks” that have been implicated in scaffolding a wider ring of additional motor proteins to increase torque, but the size of these disks is excessive for a role solely in scaffolding motor proteins. Here, we show that the basal disk is a flange that braces the flagellar motor during disentanglement of its flagellar filament from interactions with the cell body and other filaments. We show that motor output is unaffected when we shrink or displace the basal disk, and suppressor mutations of debilitated motors occur in flagellar-filament or cell-surface glycosylation pathways, thus sidestepping the need for a flange to overcome the interactions between two flagellar filaments and between flagellar filaments and the cell body. Our results identify unanticipated co-dependencies in the evolution of flagellar motor structure and cell-surface properties in the *Campylobacterota*.

INTRODUCTION

Many bacteria use flagella, membrane-embedded rotary motors connected to external helical propellers, to move through their environments.¹ All flagella, across genera separated by billions of years of evolution, share the same core proteins. A ring of motor proteins called stator complexes harness ion flux to rotate a tens-of-nanometers-wide cytoplasmic ring, or C-ring. The C-ring is connected to a chassis structure in the inner membrane called the MS-ring, which, in turn, forms the hub of an ~30-nm-long axial driveshaft (the rod) that spans the periplasm, an ~50-nm-long universal joint for torque redirection (the hook), and the multimicron-long flagellum itself.

Research has focused on the model organisms *Escherichia coli* and *Salmonella typhimurium*, which have several flagella distributed around the cylindrical sides of their rod-shaped cells.² When all flagella rotate counterclockwise (CCW), they form a coherent bundle that propels the cell. Re-orientation of the cell’s swimming trajectory (i.e., chemotaxis) occurs when one or more flagellar motor transiently changes rotational direc-

tion, which causes the cell to randomly re-orient or “tumble”; chemotaxis is achieved by inhibiting tumbling if the chemical environment is becoming more favorable to bias the otherwise random walk in beneficial directions.

The low-complexity architecture and randomized placement of flagella in these organisms, however, is only one paradigm of flagellation. Many species, including those from *Vibrio*, *Pseudomonas*, *Bdellovibrio*, *Helicobacter*, and *Campylobacter* genera, deterministically assemble motors at one or both poles. Polarly localized flagellar motors are more structurally complex than lateral flagella, featuring large periplasmic disks of unclear significance.

Polar motors preclude filament bundling as a swimming style. Swimming in bipolar-flagellated species involves wrapping the leading flagellum around the cell body to exert thrust in concert with the lagging flagellum.^{3–6} In previous work, we showed that *Campylobacter jejuni* (*C. jejuni*), a member of the *Campylobacterota* (previously epsilonproteobacteria⁷), reorients by unwrapping its wrapped leading filament from the cell surface by switching motor rotation; this allows the previously unwrapped (lagging)



filament to take its place wrapped around the cell body from the other pole. The flagella thus reverse their polarity and the cell swims away in approximately the opposite direction, whereas a non-chemotactic mutant (i.e., $\Delta cheY$) never unwraps its leading flagellum and is unable to re-orient its swimming direction. We also found that a non-helical *C. jejuni* mutant was less efficient at unwrapping its leading filament, which we attributed to increased contact between the flagellar filament and cell surface, indicating that there is an affinity between the two.

C. jejuni has one of the largest and most complex flagellar motors, featuring several periplasmic disks absent in *Salmonella*.⁸ The largest is the ~100-nm-wide basal disk, which assembles from thousands of copies of the lipoprotein FlgP.⁹ The basal disk is required for assembly of other periplasmic disks that form a scaffold required for incorporation of a wider ring of stator complexes into the motor. This wider ring of additional stator complexes is consistent with the *C. jejuni* motor producing approximately three times the torque of the *E. coli* and *Salmonella* motors.⁸ The basal disk, however, is much wider than the periplasmic scaffold and stator complex ring, and it is unclear what benefit *C. jejuni* gains from such an apparently excessively wide disk.

We speculated that the basal disk in *C. jejuni* has functions beyond just being the assembly platform for the wider stator complex ring. We recently discovered that attractive forces between the glycosylated flagellar filament and glycosylated cell body must be overcome during unwrapping of the leading filament. Here, we hypothesized that the large diameter of the *C. jejuni* basal disk is an adaptation that allows the disk to act as a flange to stabilize the high-torque *C. jejuni* flagellar motor during unwrapping. We present structural, genetic, and microscopic experiments consistent with this model.

RESULTS

Reducing disk width does not affect motor rotation

We sought to isolate the contribution of disk diameter from the requirement of the disk for a functional motor. Deletion of the genes responsible for assembly of the basal disk, *flgPQ*, prevents stator complex scaffolding and paralyzes the flagellum. To assess the significance of disk diameter, we made a mutant (EJC168) (Table 1) that constructs narrower basal disks but still enables assembly of the stator-complex periplasmic scaffold by deleting *flgPQ* from the chromosome and expressing them *in trans* from a titratable, synthetic *C. jejuni tetRA* promoter system at the *astA* locus.¹⁰ In the absence of inducer anhydrotetracycline (ATc), cells were non-motile (Figure S1A) and did not express detectable levels of FlgP. Increasing the concentration of ATc from the lowest concentration tested (12.5 ng/mL) to the highest tested (100 ng/mL) resulted in a corresponding increase of *flgP* expression (Figure 1B).

Electron cryotomography of motors from cells grown at different ATc concentrations confirmed that disk size correlated with induction level (Figures 1C and 1D). Disks were absent in the absence of ATc, as were stator complexes, equivalent to *flgP* or *flgQ* deletion.⁸ Motors assembled at low *flgPQ* expression had narrower disks but were able to assemble the periplasmic scaffold and MotAB stator complexes. Increasing *flgPQ* expression produced correspondingly wider basal disks,

with average diameters of 84, 98, and 107 nm for 25, 50, and 100 ng/mL ATc, respectively. We could discern periplasmic scaffold densities in disks as narrow as 50 nm, whereas the average wild-type (WT) motor is 105 nm but can be as wide as 130 nm.

Although disk diameter correlated with the level of *flgPQ* induction, we found broad disk diameter distributions (Figure 1D). We therefore attempted to engineer a mutant that assembles consistently narrow basal disks while remaining motile in soft agar by alanine replacement of residues in FlgP thought to be involved in basal disk construction based on our recent *in situ* high-resolution structure of the *C. jejuni* flagellar motor.⁹ We found that *flgP*^{S69A E157A K159A} (*flgP*^{AAA}) assembled disks comparable in diameter to the smallest disks found in EJC168 at low induction (25 ng/mL ATc) with less size variation (Figure 1E). Based on western-blot analysis of FlgP, we conclude that FlgP levels in *flgP*^{AAA} are reduced to a fraction of WT through an as-yet-unknown mechanism (Figures S1B–S1E). We found that basal disk diameters in *flgP*^{AAA} cluster more tightly than in the ATc induction series and never extend beyond ~80 nm in diameter (Figure 1D).

We found that motor rotation was not compromised by having a smaller disk. Across all induction levels and in the *flgP*^{AAA} background, both swimming velocity and filament rotation rate were comparable with WT cells (Figures 1F and S1F), demonstrating that motor rotation is independent of disk width beyond the minimal width required for stator complex incorporation. These data show that the WT disk diameter is excessive for a role in stator complex assembly alone, suggesting functions beyond rotation.

Cells with small basal disks autoagglutinate faster than WT

Despite small-disk motors rotating their flagella at WT speeds, we noticed that suspensions of cells grown on lower concentrations of ATc formed large clumps of cells bound together by their flagellar filaments within minutes of being applied to the sample chamber for observation, unlike suspensions of WT and high-induction cell suspensions (Video S1). This clumping, known as autoagglutination, is an adaptive behavior important for microcolony and biofilm formation during host colonization.^{11,12} Autoagglutination requires a flagellar filament, and mutants with impaired or non-functional motors autoagglutinate faster than WT (Figures 2A and S2A–S2C),

The increased autoagglutination of EJC168 at low induction and the *flgP*^{AAA} mutant is at least partially the result of functional motors with small disks and not solely due to paralyzed motors in a proportion of the population. Discrete cells trapped in aggregates are often bound to the cell clusters by filaments with rotating motors (Video S2). Additionally, although low-induction EJC168 and *flgP*^{AAA} cell suspensions have a proportion of entirely paralyzed, disk-less cells (12.5 ng ATc/mL: 9% w/disk; 25 ng ATc/mL: 35% w/disk; 50 ng ATc/mL: 75% w/disk; 100 ng ATc/mL: 88% w/disk), *flgP*^{AAA}, with a higher percentage of cells with disks (44%), all of which are small, autoagglutinates faster than EJC168 induced at 25 ng/mL ATc, which has on average fewer, but larger, disks. This result suggests that wider basal disks may be needed by motors to counteract excessive autoagglutination (Figure 2B).

Table 1. List of strains used in this study

Strain number	Genotype	Reference	Notes
EJC28	<i>flaA</i> ^{S397C}	Cohen et al ⁵	wild type (WT)
EJC168	$\Delta flgPQ \Delta P_{astA}::cat-tetR_{P_{tetA}V2} \Delta astA::flgPQ flaA$ ^{S397C}	this study	–
EJC242	<i>flgQ</i> -6xHis <i>flaA</i> ^{S397C}	this study	–
EJC243	<i>flgP</i> ^{S69A E157A K159A} <i>flgQ</i> -6xHis <i>flaA</i> ^{S397C}	this study	<i>flgP</i> ^{AAA}
EJC244	<i>flgP</i> ^{S69A E157A K159S} <i>flgQ</i> -6xHis <i>flaA</i> ^{S397C}	this study	<i>flgP</i> ^{AAS}
EJC112	<i>flgP</i> - <i>lpp</i> ³⁴ <i>flaA</i> ^{S397C}	this study	–
EJC113	<i>flgP</i> - <i>lpp</i> ⁴¹ <i>flaA</i> ^{S397C}	this study	–
EJC114	<i>flgP</i> - <i>lpp</i> ⁴⁸ <i>flaA</i> ^{S397C}	this study	–
EJC115	<i>flgP</i> - <i>lpp</i> ⁵⁵ <i>flaA</i> ^{S397C}	this study	–
EJC137	<i>flgP</i> - <i>lpp</i> ⁵⁵	this study	–
DRH2070	$\Delta flgP$	Hendrixson lab	–
EJC188	<i>flgP</i> ^{$\Delta 18-62$} <i>flaA</i> ^{S397C}	this study	–
–	<i>flgP</i> - <i>lpp</i> ⁵⁵ <i>flgG</i> ^{T54N} <i>flaA</i> ^{S397C}	this study	–
–	<i>flgP</i> - <i>lpp</i> ⁵⁵ <i>pseG</i> ^{I142T} <i>flaA</i> ^{S397C}	this study	–
–	<i>pseG</i> ^{I142T} <i>flaA</i> ^{S397C}	this study	–
EJC91	$\Delta flgPQ$	this study	–
EJC92	$\Delta flgQ$	this study	–
EJC93	$\Delta flgQ1.5$	this study	endpoint, motile isolate of first $\Delta flgQ$ evolved lineage
EJC94	$\Delta flgQ2.5$	this study	endpoint, motile isolate of second $\Delta flgQ$ evolved lineage
EJC95	$\Delta flgPQ1.5$	this study	endpoint, motile isolate of first $\Delta flgPQ$ evolved lineage
EJC96	$\Delta flgPQ2.6$	this study	endpoint, motile isolate of second $\Delta flgPQ$ evolved lineage
EJC97	$\Delta flgPQ \Delta 0661 flaA$ ^{S397C}	this study	–
EJC98	$\Delta flgPQ \Delta pglAB::aphA flaA$ ^{S397C}	this study	–
EJC99	$\Delta flgPQ \Delta kpsD flaA$ ^{S397C}	this study	–
EJC100	$\Delta flgPQ \Delta 0661 \Delta pglAB::aphA flaA$ ^{S397C}	this study	–
EJC101	$\Delta flgPQ \Delta 0661 \Delta kpsD flaA$ ^{S397C}	this study	–
EJC102	$\Delta flgPQ \Delta pglAB::aphA \Delta kpsD flaA$ ^{S397C}	this study	–
EJC103	$\Delta flgPQ \Delta 0661 \Delta pglAB::aphA \Delta kpsD flaA$ ^{S397C}	this study	–
EJC104	$\Delta flgPQ \Delta 0661 \Delta pglAB::aphA \Delta kpsD \Delta flaAB::flaA$ ^{S397C}	this study	all-FlaA filament
EJC105	$\Delta flgPQ \Delta 0661 \Delta pglAB::aphA \Delta kpsD \Delta flaAB::flaB$ ^{S397C}	this study	all-FlaB filament
EJC106	$\Delta flgPQ fligG$ ^{G305S}	this study	–
EJC107	$\Delta flgPQ \Delta flaAB::flaB$ ^{S397C/T4771}	this study	all-FlaB ^{T4771} filament
EJC108	$\Delta flgPQ \Delta flaAB::flaB$ ^{S397C/T4771} <i>fligG</i> ^{G305S}	this study	–
EJC109	$\Delta 0661 flaA$ ^{S397C}	this study	–
EJC255	$\Delta waaF flaA$ ^{S397C}	this study	–
EJC256	$\Delta waaF flgP$ - <i>lpp</i> ⁵⁵ <i>flaA</i> ^{S397C}	this study	–
EJC257	$\Delta kpsM::cat flaA$ ^{S397C}	this study	–
EJC258	$\Delta kpsM::cat flgP$ - <i>lpp</i> ⁵⁵ <i>flaA</i> ^{S397C}	this study	–
EJC259	$\Delta pglAB::aphA flgP$ - <i>lpp</i> ⁵⁵ <i>flaA</i> ^{S397C}	this study	–
EJC261	$\Delta 0661 flgP$ - <i>lpp</i> ⁵⁵ <i>flaA</i> ^{S397C}	this study	–
EJC263	$\Delta kpsD flgP$ - <i>lpp</i> ⁵⁵ <i>flaA</i> ^{S397C}	this study	–
EJC266	$\Delta 0661 \Delta pglAB::aphA \Delta kpsD flgP$ - <i>lpp</i> ⁵⁵ <i>flaA</i> ^{S397C}	this study	–

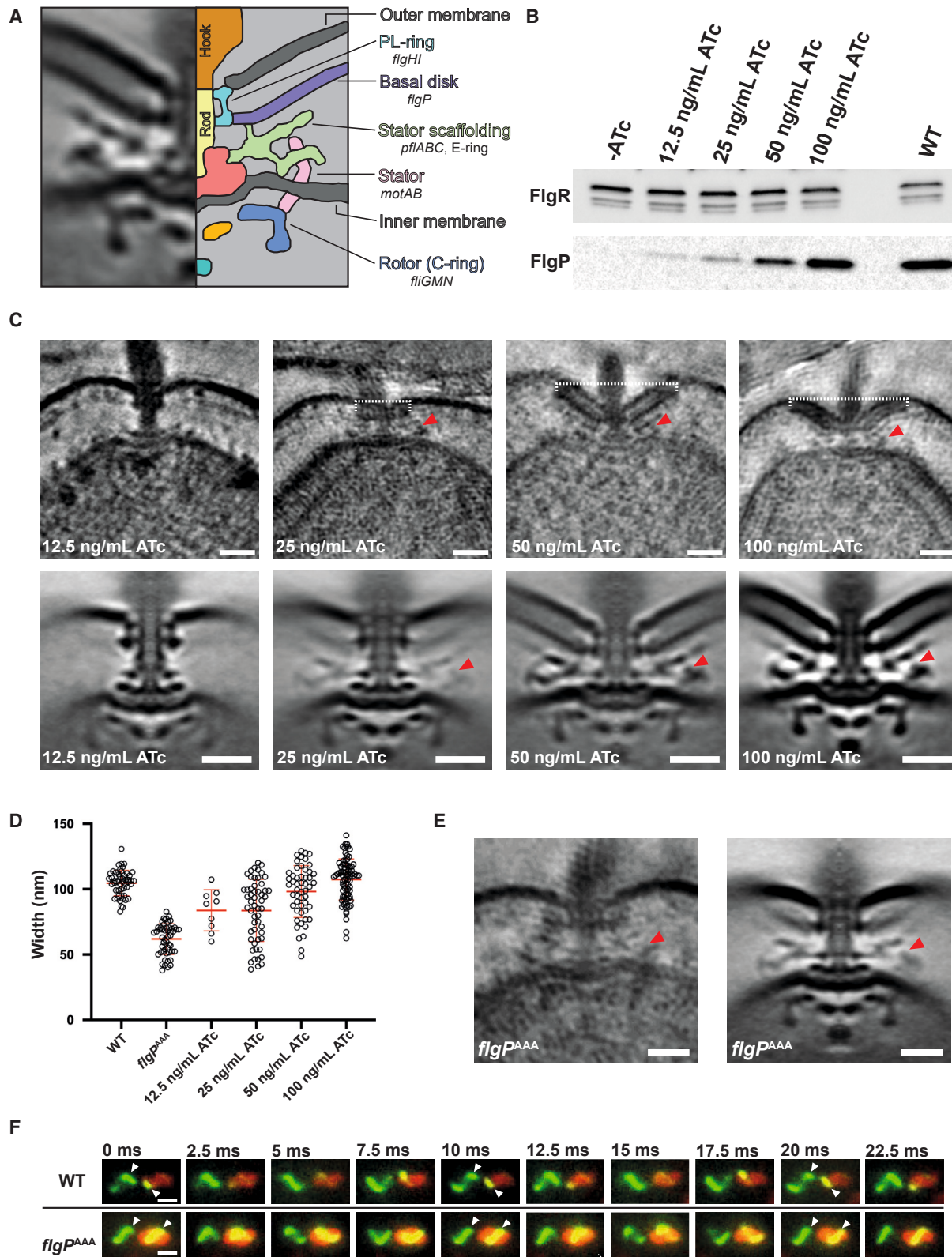


Figure 1. Engineered motors with small basal disks nevertheless incorporate stator complexes and rotate similarly to WT motors

(A) The flagellar motor of *Campylobacter jejuni* has the same components as that of the model organisms, as well as extra embellishments such as the basal disk and stator scaffolding architecture.

(legend continued on next page)

The basal disk must be in register with the P-ring for effective motility

That motors with small disks may cause excessive autoagglutination suggested to us that the disk might act as a mechanically reinforcing flange to stabilize the high-torque *C. jejuni* motor to overcome immediate autoagglutination when near other cells. The basal disk polymerizes around the P-ring, which is believed to act with the L-ring as a non-rotating bushing to brace the rotating flagellar driveshaft. We reasoned that we could test this model by shifting the basal disk out of register with the P-ring, disrupting mechanical support of the P-ring by the basal disk, yet preserving the disk's role in stator scaffolding.

We engineered FlgP mutants to push the disk out of register with the P-ring. FlgP is a small protein with an N-terminal cysteine (C17), presumed to be lipoylated and inserted in the inner leaflet of the outer membrane (OM). A poorly conserved N-terminal ~40 residues of the mature protein is likely to be a linker anchored to the OM by C17. This is supported by an ~6-nm unresolved gap between the OM and basal disk in the subtomogram average structure of the *C. jejuni* motor, a distance consistent with an ~40-residue linker. To displace the disk, we inserted heptad repeats of varying length from the *Salmonella* lipoprotein LppA (also known as Braun's lipoprotein) downstream of C17 (Figure 3A), followed by the native FlgP OM-linker sequence, based on previous success using Lpp to alter spacing in the periplasm.^{13–15} These mutants were motile in soft agar, but motility decreased as more heptads were added (Figures S3A–S3C). We chose the mutant that formed the smallest swarm in soft agar but was nevertheless still motile, *flgP-lpp*⁵⁵, for further analysis.

Subtomogram averaging confirmed that the *flgP-lpp*⁵⁵ motor had a basal disk that had been shifted out of register with the P-ring by ~7–8 nm, consistent with the 8.4 nm expected by insertion of a 55-residue α helix (Figure 3B). In this mutant, the disk encircles the proximal rod instead of the P-ring. Curiously, the disk appears to self-assemble non-specifically around whichever axial component it is in register with, as the inner radius of the *flgP-lpp*⁵⁵ disk (Figure 3B red dashed line) was narrower than the WT disk, matching the decreased width of the structure around which it was assembling (i.e., the rod rather than the wider P-ring). Although *flgP-lpp*⁵⁵ forms small-diameter swarms in soft agar (Figure 3C), the stator scaffolding architecture in the *flgP-lpp*⁵⁵ motor was indistinguishable from the WT motor, and three-dimensional (3D) holographic tracking microscopy of the *flgP-lpp*⁵⁵ mutant swimming in viscous media revealed a subset of the population swimming at WT velocity (white

arrowheads in Figure 3D), indicating that motors with basal disks displaced from around the P-ring could still function as well as WT. Together, these results demonstrate that the poor motility of the *flgP-lpp*⁵⁵ mutant in soft agar is not due to impairment of motor rotation.

To determine how displacement of the basal disk reduced motility in soft agar despite the presence of motile cells in liquid media, we labeled the flagellar filament with fluorescent dye and recorded swimming by high-speed video fluorescence microscopy. As with our small-disk mutants, and consistent with our holographic tracking, flagellar rotation rate in the *flgP-lpp*⁵⁵ mutant was comparable with WT, but the mutant was incapable of unwrapping the leading flagellum from the cell body during motor reversals (Video S3, top). Consequently, the *flgP-lpp*⁵⁵ mutant exhibited a stuttering motility characterized by short runs interrupted by brief pauses with no net change in swimming trajectory (Figure 3E), as well as doubly wrapped cells (Video S4), phenotypes that were reminiscent of the defective-unwrapping phenotype we observed by high-speed fluorescence video in non-helical mutants of *C. jejuni* in one of our previous studies.⁵ This is in contrast to WT cells, which have a swimming style referred to as darting motility, whereby chemotaxing cells change swimming trajectory during motor reversals due to the wrapping and unwrapping of the opposed flagellar filaments (Video S3, bottom), and where we have never seen doubly wrapped cells.

Thus, the phenotype of the *flgP-lpp*⁵⁵ mutant in soft agar reflects the inability of the filament to be pulled from the cell body during motor switching across the entire population. We used low-magnification darkfield microscopy and *C. jejuni*'s tendency to migrate toward regions of higher oxygen (a.k.a. aerotaxis) to visualize how the failure to unwrap in the *flgP-lpp*⁵⁵ background manifested at the population level, as in our previous work.⁵ This showed that the failure of *flgP-lpp*⁵⁵ to unwrap upon motor reversal results in population-level failure to swarm toward regions of higher oxygen content, unlike WT populations (Video S5).

To understand how this impairment would affect motility in environments like those of the mucous-filled gastric crypts of a host's digestive tract, we observed fluorescently labeled cells swimming through viscous media in a microfluidic device with confined 1 μ m channels, allowing only one cell through at a time. Although individual *flgP-lpp*⁵⁵ cells were able to traverse the device at the same speed as WT cells (Figures 3F and 3G), further confirming our findings from subtomogram averaging and 3D holographic cell tracking that the function of the

(B) Increasing the level of ATc in the growth medium corresponded to an increased level of *flgP* expression. FlgR antisera was used as an internal loading control. (C and D) (C) Slices of individual tomograms (top) and subtomogram averages (bottom) (scale bars, 20 nm) of motors at different *flgP* expression levels and (dashed white lines indicate width measurement, stators [MotB] are incorporated into the motor even under low-induction conditions [red arrowheads]). (D) Measurements of basal disk widths of individual motors in electron cryo-tomograms (disk widths are significantly different between WT, *flgP*^{AAA}, and EJC168 at 25 and 50 ng/mL ATc, one-way ANOVA and two-tailed t tests, $p \leq 0.0001$ – 0.0385 , bars represent mean \pm SEM). In the WT, all the motors imaged possessed basal disks, whereas in EJC168, lower concentrations of ATc corresponded to a lower proportion of motors with disks. Disk-less motors were excluded from the analysis in (D).

(E) The *flgP*^{S69A E157A K159A} (*flgP*^{AAA}) mutant constructed small-diameter basal disks, and the distribution of basal-disk diameters clustered more tightly than EJC168 at all induction levels and never extended beyond ~80 nm (left: slice through a single tomogram; right: subtomogram average of FlgP^{AAA} motor [scale bars, 20 nm]).

(F) Still frames of high-speed video of fluorescently labeled WT and *flgP*^{AAA} cells (scale bars, 1 μ m). The position of filaments relative to the cell body (white arrowheads) can be used to approximate rotation rate. For both the WT and *flgP*^{AAA}, rotation rate was found to be ~100 Hz (1 revolution/10 ms). See also Videos S1 and S2.

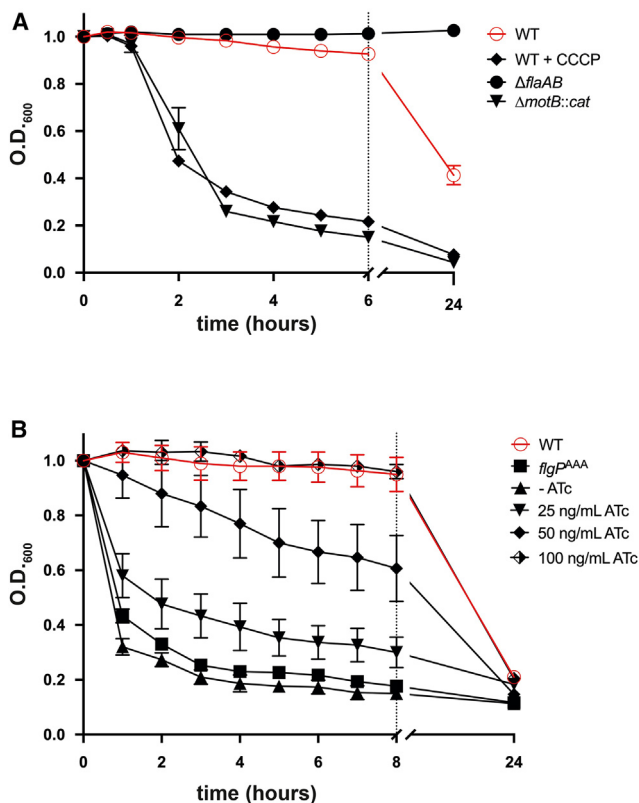


Figure 2. Low FlgP expression and mutation of FlgP enhance autoagglutination

(A) A flagellar filament is required for autoagglutination, and a functional motor prevents excessive autoagglutination. The sedimentation rates (i.e., autoagglutination) of a suspension of WT cells paralyzed with CCCP or a paralyzed mutant ($\Delta motB::cat$) are significantly faster than the non-treated cell suspension (two-tailed t test, $p = 0.0062$).

(B) Low FlgP expression in EJC168 corresponded to a faster sedimentation rate. The $flgP^{AAA}$ mutant sedimented significantly faster than EJC168 induced with 25 ng/mL ATc (two-way ANOVA, $p \leq 0.0001$, error bars are mean \pm SEM). See also Videos S1 and S2.

torque-generating motor core is unaffected by displacing the disk, the displaced-disk $flgP-lpp^{55}$ mutant was unable to reverse direction when encountering obstacles (i.e., immobilized cells) in the channel, leading to *C. jejuni* pileups (Video S6). In contrast, WT cells reversed direction upon encountering an obstacle and exited the device (Figure S3D; Video S7). We next inoculated day-old chicks with identical numbers of WT, $\Delta flgP$ or $flgP-lpp^{55}$ cells and enumerated the number of colony-forming units (CFUs) in the ceca of the chicks at 1 week post inoculation. As predicted by our microfluidic device results, we found that the $flgP-lpp^{55}$ mutant colonized the chicken cecum as poorly as the non-motile $\Delta flgP$ control strain (Figure 3H). These results show that, in addition to the basal disk's role in stator scaffolding, flanging of the motor by the basal disk is an important adaptive trait for *C. jejuni* in its native environments.

We also produced a mutant in which the disk was moved closer to the OM, and out of register with the P-ring, by deletion of the OM-linker while retaining C17 ($flgP^{\Delta 18-62}$). In soft agar, $flgP^{\Delta 18-62}$ produced a swarm $\sim 30\%$ that of WT (Figure S3E). In

contrast to $flgP-lpp^{55}$, however, the subtomogram average of the $flgP^{\Delta 18-62}$ motor had poorly resolved stator scaffolds, suggesting that the motility defect in this background is likely due to disruption of motor assembly and consistent with FlgP being too far from the inner membrane to template formation of the periplasmic scaffold (Figure S3F).

We conclude that a wide disk is required for overcoming filament-filament (self-other) interactions during autoagglutination, while a correctly positioned disk is required to act as a flange to overcome filament-cell (self-self) interactions during unwrapping.

Mutations that restore motility to a displaced-disk mutant suggest a link between filament unwrapping and filament glycosylation

Suppressing mutations in the $flgP-lpp^{55}$ background that restored near-WT levels of motility arise following 36–48 h of incubation in soft agar, appearing as flares emanating from the original, poor-motility swarm. Reasoning that the identity of the suppressor mutations would provide further information regarding the function of the basal disk, we isolated two independent revertants, performed whole-genome sequencing, and found two paths to suppress the $flgP-lpp^{55}$ motility defect: restoration of the P-ring/basal disk register (i.e., restoration of flanging), or decreased O-glycosylation of the flagellar filament (Figure S4A).

The first motile revertant of $flgP-lpp^{55}$ acquired a point mutation in the distal rod gene, $flgG^{T54N}$. In WT flagellar motors, the distal rod only grows long enough for a single P-ring and a single L-ring before it contacts the OM and stops polymerizing, but alleles in $flgG$ have been isolated in *Salmonella* that allow the distal rod to continue polymerizing once it reaches the OM.¹⁶ These so-called $flgG^*$ alleles often arise in an N-terminal region of FlgG known as the Dc domain, encompassing residues ~ 30 –70 of the protein.^{17–19} Similarly, our $flgG^{T54N}$ allele allows the distal rod to grow longer than usual to accommodate two P-rings around the distal rod (Figure 4A); thus, the additional space imposed by the Lpp⁵⁵ insertion is compensated for by an additional P-ring on $flgG^{T54N}$, thus restoring register of the first P-ring to the basal disk while the second P-ring templates assembly of the L-ring for correct OM-penetration and hook/filament assembly. In addition to suppressing the motility defect of the $flgP-lpp^{55}$, the $flgG^{T54N}$ allele also suppressed the moderate autoagglutination defect of the $flgP-lpp^{55}$ mutant (Figure 4D), indicating that flanging of the P-ring by the basal disk is also important for preventing excessive autoagglutination.

The second revertant was intriguing because the suppressing mutation, $pseG^{142T}$, affects the flagellar filament rather than the motor. PseG is a uridine-diphosphate-sugar (UDP-sugar) hydrolase involved in the synthesis of pseudaminic acid (PseAc),^{20,21} the O-linked sugar that decorates the flagellar filament at 19 serine and threonine residues of each flagellin monomer in *C. jejuni* 81–176.^{22–24} Glycosylation of the flagellar filament in *C. jejuni* is required for both filament assembly as well as autoagglutination, but only three of the 19 glycosylable flagellin residues are critical for filament assembly and motility, and a $pseG$ knockout is non-motile.^{25,26} We therefore reasoned that substitution of a non-polar isoleucine residue adjacent to the substrate-binding site of PseG with a threonine, decreases, but must not abolish, its enzymatic

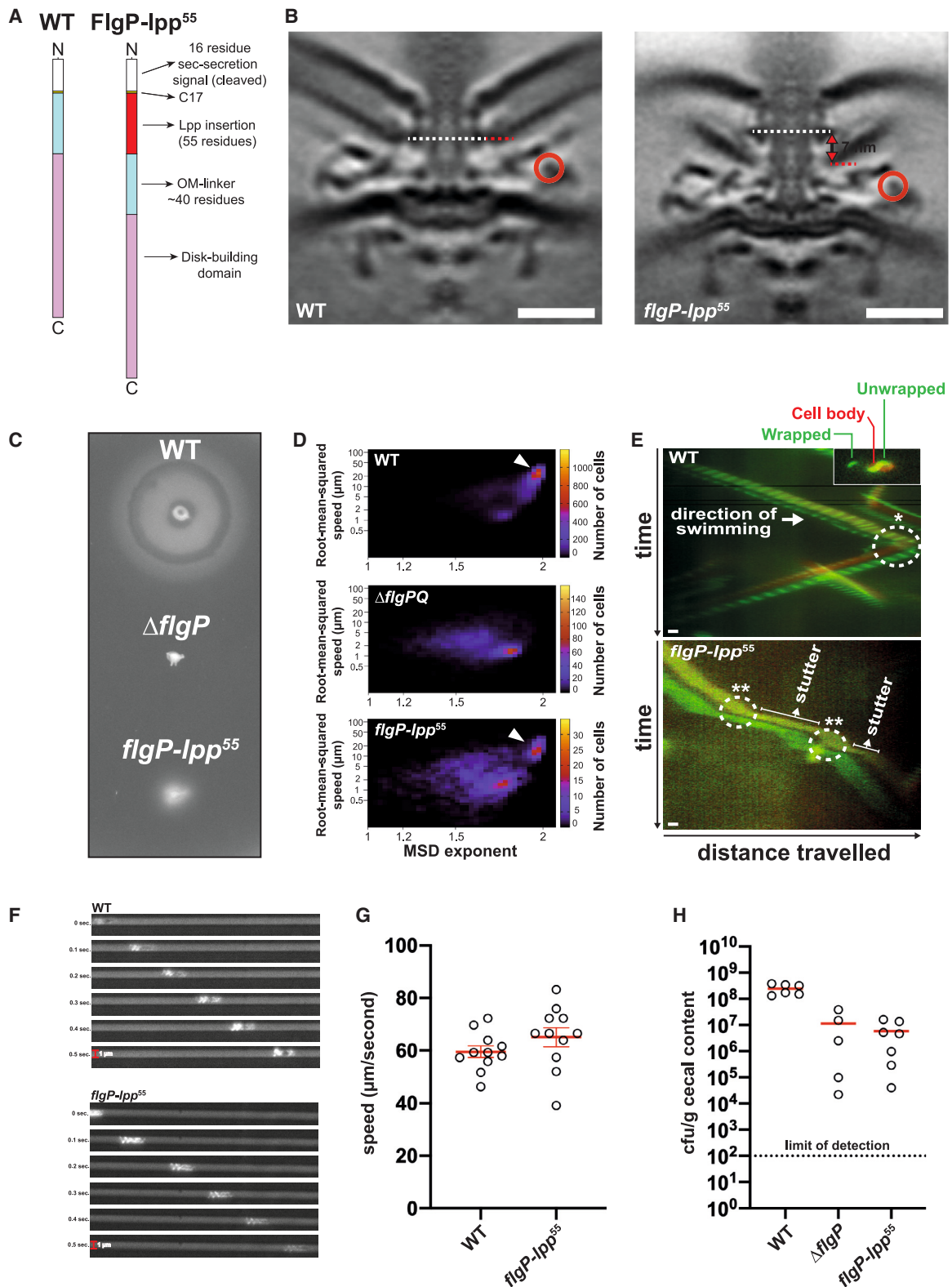


Figure 3. Displacement of the basal disk from the P-ring reduces filament unwrapping

(A) A 55-residue segment from *Salmonella* LppA (also known as Lpp or Braun's lipoprotein) was inserted after C17 in FlgP to make FlgP-*lpp*⁵⁵.

(B) Subtomogram averaging of the *flgP-lpp*⁵⁵ mutant's motor revealed that the basal disk had been displaced from the P-ring by ~7 nm (P-ring: white dashed line, first ring of basal disk: red dashed line) and had a narrower first ring of FlgP subunits but that stator recruitment was not impacted (red circles) (scale bars, 20 nm).

(legend continued on next page)

activity and results in filaments with reduced or altered *O*-glycosylation. This interpretation is supported by the observation that while the *pseG*¹⁴² allele in an otherwise WT background has no effect on swarm diameter in soft agar or flagellar filament length (Figures 4B, 4C, and S5A), the flagellin in a *pseG*^{142T} background migrates differently by isoelectric-focusing gel electrophoresis, indicating it has altered glycosylation (Figures S5B and S5C). Furthermore, the *pseG*^{142T} allele significantly reduces autoagglutination in both the WT and *flgP-lpp*⁵⁵ backgrounds (Figure 4D) (two-way ANOVA, $p \leq 0.0001$, error bars represent SEM), in agreement with previous work showing that eight of 19 glycosylated flagellin residues are important for autoagglutination.²²

When we observed the *flgP-lpp*⁵⁵ *pseG*^{142T} double mutant by high-speed video fluorescence microscopy, we found that the double mutant unwrapped its filament from the cell body during directional reversals at rates comparable with WT, in contrast to *flgP-lpp*⁵⁵ (Figure 4E). Furthermore, in both aerotaxis assays and microfluidic experiments the *flgP-lpp*⁵⁵ *pseG*^{142T} mutant exhibited near-WT behavior (Figure 4F). Consistent with our previous study showing interaction between the flagellar filament and cell body,⁵ these data implicate *O*-glycosylation of the flagellar filament in filament-cell body interactions in addition to filament-filament autoagglutination and filament assembly.

We generated knockouts of the capsular polysaccharide (CPS) genes *kpsM* and *kpsD*,²⁷ as well as a gene involved in synthesis of lipooligosaccharide (LOS), *waaF*,²⁸ to try to identify what the filament interacts with on the cell surface (Figures S5D and S5E). Whereas deletion of CPS reduced motility in both the WT and *flgP-lpp*⁵⁵ background in soft agar, deletion of *waaF* had a small but significant suppressing effect on the motility of *flgP-lpp*⁵⁵ in soft agar ($p = 0.016$, two-tailed t test). The *waaF* knockout also had an unusual phenotype in soft agar in which the main swarm is surrounded by a larger, ghostly swarm, suggesting that loss of LOS may potentiate suppression of the *flgP-lpp*⁵⁵ mutant. We speculate that the filament-cell-surface interaction is a complex interaction between multiple glycan moieties on the cell surface, but this will require further investigation.

Swimming without a basal disk requires de-glycosylation of the cell surface

Although deletion of *flgPQ* produces a non-motile phenotype in motility agar, observing this mutant by fluorescence microscopy revealed occasional cells with rotating flagella. Thus, even in the absence of the basal disk, stator complexes can still be inefficiently recruited to the motor. Given that we were able to isolate suppressors of disk displacement, we speculated that we might be able to isolate a suppressor strain of a wholesale *flgPQ* deletion that would shed more light on the role of the basal disk.

We selected for suppression of the *ΔflgPQ* motility defect through prolonged incubation in motility agar, as previous attempts over smaller time frames (~48–72 h) had been unsuccessful in isolating motile revertants. We independently inoculated two colonies each of *ΔflgPQ* and *ΔflgQ* mutants in motility agar and incubated the plates for 4–6 days. Although each colony had a non-motile phenotype after 2 days of incubation, all four isolates had speckles emanating from the site of inoculation within 5 days.

The speckled phenotype occurs when the majority of cells in motility agar are non-motile, with occasional cells possessing a functional flagellum. Upon division, these motile cells deposit non-motile daughter cells that seed colonies of non-motile descendants.²⁹ As this process occurs around the site of inoculation, the swarm takes on a speckled, or “bushy,” phenotype. After 4–6 days of incubation, the edge of each bushy swarm was picked from the agar, single-colony purified, stored at –80°C, and also used to inoculate a fresh motility plate. This process was repeated four to five times for each lineage, at which point all lineages had evolved a non-bushy swarm phenotype in soft agar (Figure 5A), indicating that the majority of cells in the population are swimming. We then performed whole-genome sequencing of each endpoint isolate for each of the four lineages to determine the mutations required for motility in the absence of the basal disk.

We predicted that disk-less motility would require mutations in flagellar genes, specifically periplasmic scaffold genes and/or the stator complex genes *motAB*, as such mutations might enable stable incorporation of stator complexes despite the lack of FlgP. To our surprise, however, the theme across all four evolved lineages was a similar constellation of spontaneous mutations in genes involved, or implicated, in decorating the cell surface with polysaccharides (Table 2). Each lineage had mutations in the *pgl* operon, responsible for *N*-glycosylation of a diverse cohort of periplasmic and surface-exposed proteins.^{30–33} A further two lineages had spontaneously acquired mutations in *kps* genes, which are responsible for CPS biogenesis.²⁷ Additionally, mutations in a gene predicted to function as a polysaccharide deacetylase, *cjj_81-176_0661* (hereafter referred to as *O661*) were present in all four evolved lineages. Each lineage also had evidence of phase variation in *kps*-associated sugar transferase and CPS-modification genes.^{34,35}

In addition to mutations in genes involved or implicated in decoration of the cell surface with sugars, two of the isolates had single-nucleotide polymorphisms (SNPs) in the gene encoding the cytoplasmic rotor, *fliG*,³⁶ and one isolate had a second flagellar mutation at the *fla* locus: *ΔflaA::flaB*^{T4771}, in which the WT flagellin locus encoding both the major flagellin *flaA* and

(C and D) (C) Following overnight incubation in soft agar, the *flgP-lpp*⁵⁵ mutant formed small-diameter swarms in motility agar compared with WT, despite (D) the presence of a population of cells swimming at WT velocity when cell suspensions were observed by 3D-holographic-tracking microscopy (arrowheads).

(E) Kymographs generated from high-speed fluorescence video show that the *flgP-lpp*⁵⁵ mutant is incapable of unwrapping its filament from the cell body during motor reversals and does not change swimming direction, as opposed to the characteristic darting motility of WT *C. jejuni* where unwrapping leads to a reversal of swimming direction. Single asterisk: unwrapping of leading filament and wrapping of lagging filament; double asterisk: failure to unwrap (scale bars, 1 μm).

(F and G) The velocity of individual *flgP-lpp*⁵⁵ cells traversing a microfluidic device with 1-μm-wide channels was found to be identical to WT (two-tailed t test, $p = 0.212$, bars represent mean ± SEM), confirming our observations from holographic tracking, although *flgP-lpp*⁵⁵ cells fail to reverse upon encountering obstacles.

(H) The *flgP-lpp*⁵⁵ mutant has a significant host colonization defect relative to WT, colonizing the chicken cecum as poorly as a non-motile *ΔflgP* mutant (one-way ANOVA, $p \leq 0.0001$, bars represent mean CFU/g cecal content).

See also Videos S3, S4, S5, S6, and S7.

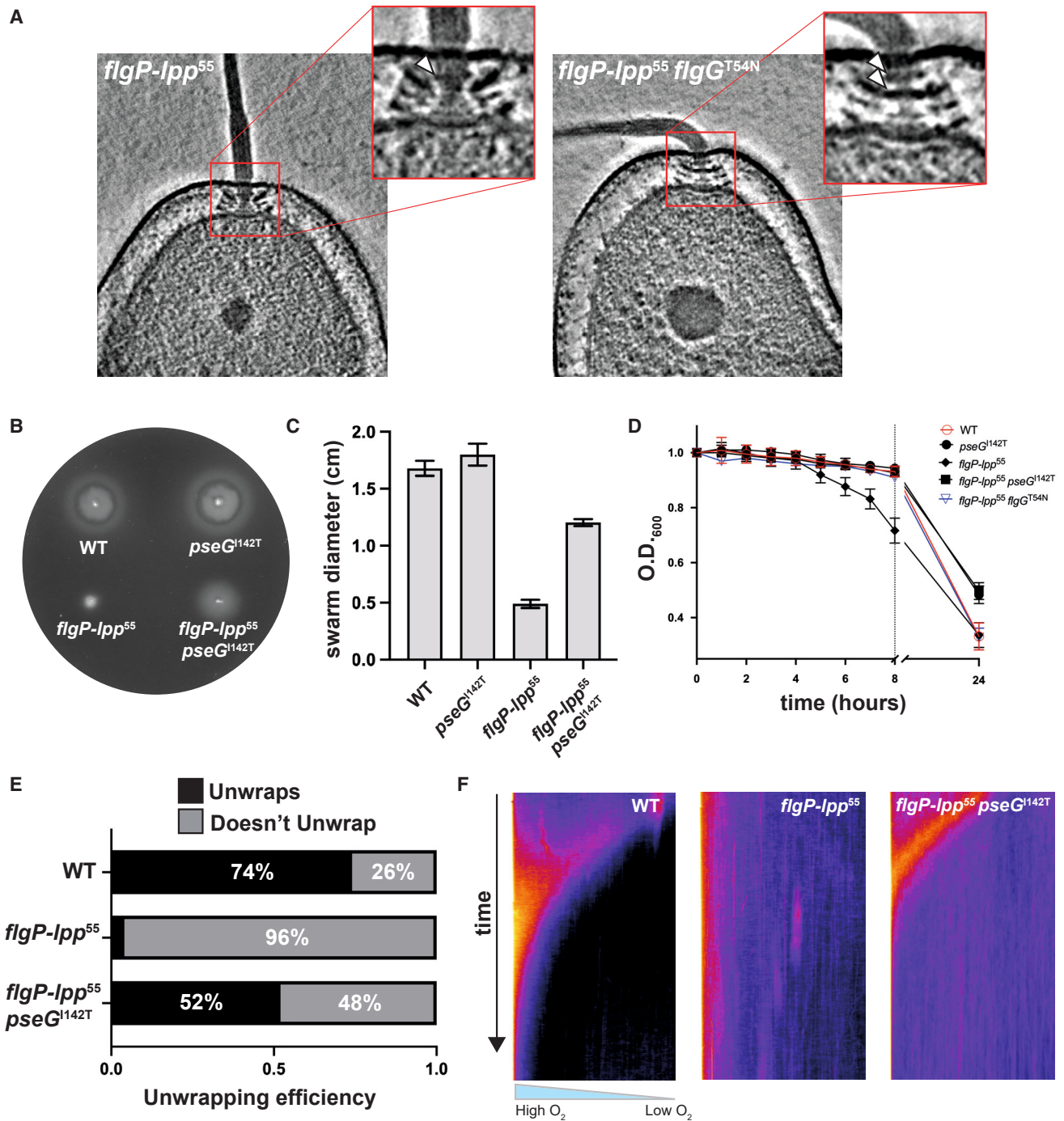


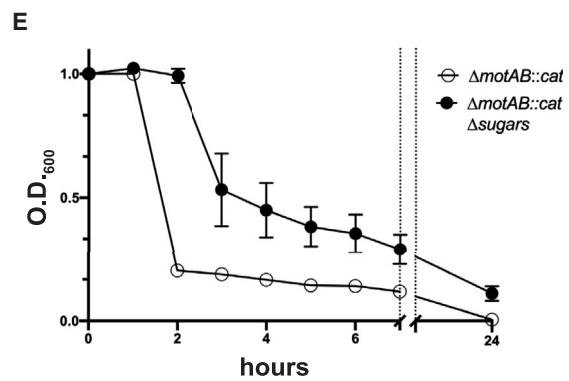
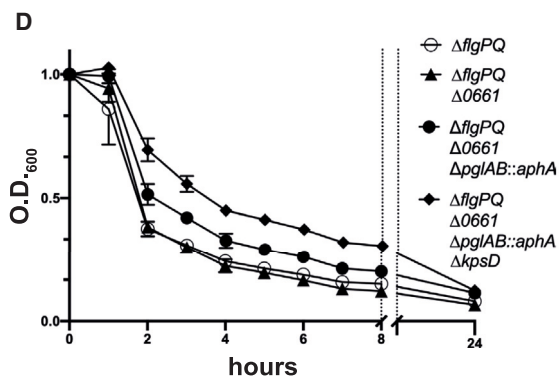
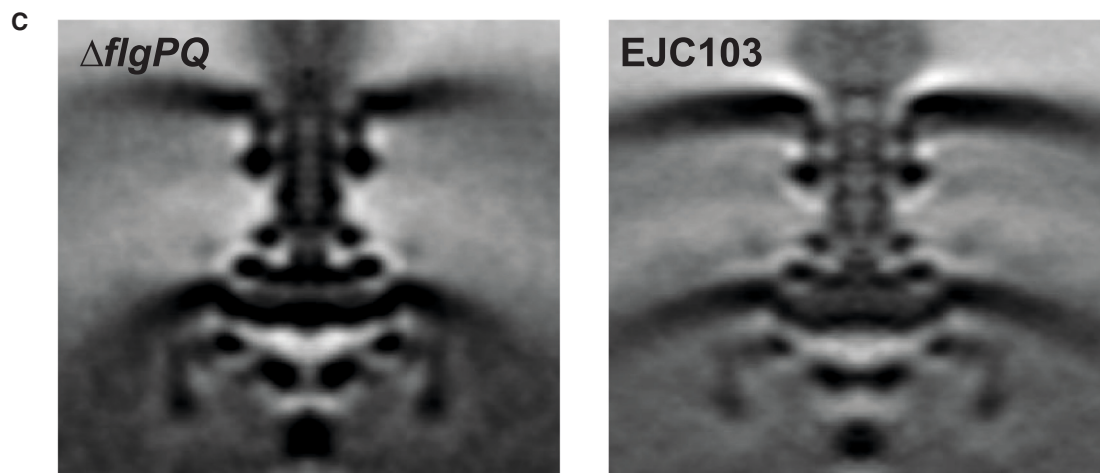
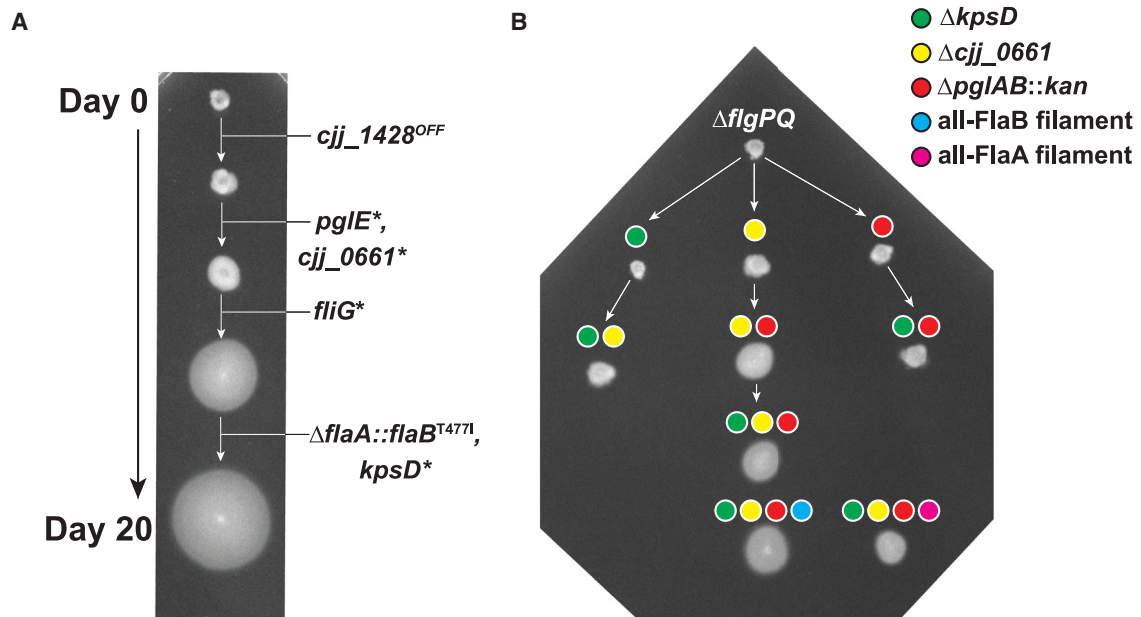
Figure 4. Suppression of the *flgP-lpp*⁵⁵ motility defect occurs by restoring the basal disk P-ring register or reducing filament glycosylation
(A) The *flgG*^{T54N} allele allows the distal rod to grow longer in order to accommodate a second P-ring (arrowheads), restoring flanging of the motor by the basal disk in the *flgP-lpp*⁵⁵ background.

(B and C) The second suppressor we isolated arose in *pseG*, a UDP-sugar hydrolase involved in O-glycosylation of the flagellar filament. The *pseG*^{I142T} allele has no effect on motility in an otherwise WT background but increases soft-agar motility of the *flgP-lpp*⁵⁵ mutant.

(D) The decreased sedimentation rate caused by the *pseG*^{I142T} allele in both the WT and *flgP-lpp*⁵⁵ backgrounds indicates lower levels of O-glycosylation of the filament. Restoration of the P-ring/basal disk register in the *flgG*^{T54N} background suppressed the autoagglutination defect of *flgP-lpp*⁵⁵.

(E) Observing multiple motor switching events by high-speed video microscopy revealed that the *pseG*^{I142T} allele suppresses the *flgP-lpp*⁵⁵ motility defect by enabling unwrapping of the filament from the cell body upon motor reversal. (31/42 [74%] switches led to unwrapping in WT, 2/45 [4%] in *flgP-lpp*⁵⁵, and 22/42 [52%] in *flgP-lpp* *pseG*^{I142T}).

(F) The increased unwrapping conferred by the *pseG*^{I142T} suppressor is demonstrated at the population level by the restored aerotactic behavior of the *flgP-lpp*⁵⁵ *pseG*^{I142T} double mutant toward a region of higher O₂ concentration.



(legend on next page)

the minor flagellin *flaB* collapsed into one *flaB*-type gene expressed from the *flaA* promoter. To determine the impact of each mutation identified by whole-genome sequencing on suppression of the $\Delta flgPQ$ motility defect, we selected the endpoint, motile isolate from one lineage, EJC96, for further study as it possessed mutations in *pgl*, *0661*, and *kps* genes as well as the *fliG*^{G305S} and $\Delta flaA::flaB$ ^{T4571} alleles (Table 2).

We sequenced each gene in which a potentially suppressing allele arose at each stored time point of the EJC96 lineage to determine the order in which each suppressing allele arose. We found that loss-of-function mutations arose in *0661* and *pglE* first, followed by the *fliG*^{G305S}, $\Delta flaA::flaB$ ^{T4571}, and *kpsD** alleles (Figure 5A).

To rule out the possibility that the mutations in EJC96 that affect glycosylation were gain-of-function mutations, i.e., to confirm that the suppressing effect of the mutations on motility in soft agar was due to the loss of glycosylation, we constructed strain EJC103 ($\Delta pglAB::aphA \Delta kpsD \Delta 0661$), which lacks CPS and the ability to *N*-glycosylate proteins as well as *0661*. We found that EJC103 had a non-bushy swarm phenotype in soft agar, confirming that suppression of the $\Delta flgPQ$ motility defect occurs via loss of glycosylation. By constructing deletions of *pglAB*, *kpsD*, and *0661* in all combinations (EJC97-103, Figure 5B), we discovered that loss of *0661* is necessary for soft-agar motility in the $\Delta flgPQ$ background, as the *pglAB::aphA* and $\Delta kpsD$ alleles, either alone or in tandem, are insufficient to promote swimming in the absence of the basal disk.

To assess the importance of the *fliG*^{G305S} and $\Delta flaA::flaB$ ^{T4771} mutations relative to the glycosylation genes, we reconstituted the *fliG*^{G305S} and $\Delta flaA::flaB$ ^{T4771} mutations singly and in combination in the $\Delta flgPQ$ parental background. We found that neither *fliG*^{G305S} nor $\Delta flaA::flaB$ ^{T4771} alone suppress the $\Delta flgPQ$ motility defect, whereas the double mutant displays some degree of speckling but is otherwise indistinguishable from the $\Delta flgPQ$ parental strain (not shown). These results show that loss of cell-surface glycosylation and loss of *661* activity is necessary and sufficient to permit swimming in the absence of a basal disk, whereas flagellar-specific mutations only serve to enhance motility once the cell surface has been de-glycosylated.

To investigate the possibility that loss of *pglAB*, *kpsD*, and *0661* had somehow restored stator scaffolding in the absence of the basal disk, we performed subtomogram averaging of the $\Delta flgPQ$ and EJC103 motors and found them to be indistinguishable from one another, with no visible stator complex densities in either, (Figure 5C) as seen with subtomogram average structures

of the *Salmonella* and *E. coli* motors that lack statically assembled stator complexes.

The autoagglutination profiles from the $\Delta flgPQ$ parental strain through to EJC103 revealed that the evolution from immotile to the non-bushy swarm phenotype in motility agar coincided with a decrease in sedimentation rate (i.e., autoagglutination) (Figure 5D). Taken together, this indicates that, in the absence of a basal disk and stator scaffolding, *C. jejuni* stator complexes can still transiently incorporate into the motor to generate torque but that motility in WT cells is halted due to immediate autoagglutination. Short of the highly improbable *de novo* evolution of a replacement for *flgPQ*, the only way to restore motility is via reduction of autoagglutination by disabling cell-surface glycosylation, thereby allowing motile $\Delta flgPQ$ cells to avoid or escape cell aggregates and remain free swimming

DISCUSSION

We sought to understand the selective advantage of the large basal disk in *C. jejuni*. Our findings reveal that the complex architecture of the *C. jejuni* flagellar motor has roles in addition to simply increasing the torque of the motor and ensuring high stator occupancy and highlight the evolutionary complexity of retaining the two opposed functions of motility and autoagglutination.

Taken together, our results implicate the basal disk as a flange that stabilizes the motor, enabling the motor to function despite the filament-filament and filament-cell attractions involved in autoagglutination and flagellar wrapping around the cell body, respectively. Our small-disk mutants indicate that a small disk is sufficient to assemble a functional motor whose rotary function is unaffected. A large-diameter, properly positioned disk, while not necessary for motor rotation, seems to be critical for wrenching filaments from one another and from the cell body. We propose that this wrenching requires that the PL-ring bushing around the rod be stabilized more than it is in the model organisms *E. coli* and *Salmonella*. This is graphically illustrated by poor unwrapping when the disk is displaced from the P-ring (by insertion of Lpp in FlgP) and restored unwrapping when a P-ring is placed back in register with the disk (by a *flgG** suppressor mutation). The motility impairment arising from small disks or displaced disks can be countered by attenuating sugar-mediated interactions, with both mutants in *O*-glycosylation pathways of the flagellar filament and *N*-glycosylation pathways of the cell surface restoring motility in disk mutants.

C. jejuni coordinates its opposing flagella at each pole by wrapping the leading filament around the cell body. In WT cells,

Figure 5. Motility in the absence of a basal disk requires de-glycosylation of the cell surface

- (A) Four independent disk-less cultures were inoculated into soft agar and allowed to incubate for extended periods of time. Speckles emanating from the point of inoculation were picked, purified, stored, and also used to inoculate a subsequent prolonged incubation in soft agar. After repeating four to five times for each independent lineage, all four lineages had evolved a non-bushy swarm phenotype in soft agar.
- (B) Generating *pgl*, *kps*, and *0661* knockouts singly and in combination revealed that the sugar SNPs were loss-of-function mutations and that both loss *0661* and *N*-glycosylation (i.e., *pgl*) are required to suppress the $\Delta flgPQ$ motility defect.
- (C) Comparison of the subtomogram average structures of the $\Delta flgPQ$ and EJC103 mutants' motors confirmed that motility in the evolved disk-less mutants was not due to restoration of stator scaffolding in the motor.
- (D) Suppression of the non-motile phenotype in the absence of the basal disk corresponded with decreased sedimentation rate upon removal of *pgl* and *kps* surface polysaccharides in autoagglutination assays.
- (E) Comparison of the sedimentation rates of cells paralyzed by deletion of the stators ($\Delta motAB::cat$) in both the WT background and the $\Delta 0661 \Delta pglAB::aphA \Delta kpsD$ background shows that the decreased sedimentation rate of the of EJC103 in (D) is not a result of increased motility in this background (error bars represent mean \pm SEM).

Table 2. Suppressing alleles of the Δ flgP(Q) motility defect

	<i>Cji_81176_0661</i>	<i>pgl</i>	<i>kps</i>	Phase variation	<i>flgG</i>	<i>flaAB</i>
Δ flgQ-1	frameshift insertion: A ⁸ →A ⁹ at codon 322	<i>pglH</i> : multiple SNPs	-	<i>Cji_81176_1435</i> (CPS MeOPN transferase): frameshift deletion: C ⁹ →C ⁵ On→Off	-	-
Δ flgQ-2	transition: TAA→CAA at terminator for <i>Cji_81176_0660</i> (<i>ilvC</i>); results in <i>ilvC-0661</i> translational fusion	<i>pglB</i> : frameshift deletion: A ⁸ →A ⁷ at codon 687	<i>kpsS</i> : frameshift deletion: T ⁸ →T ⁷ at codon 35	<i>Cji_81176_1432</i> (<i>maf7</i> , putative sugar transferase): frameshift deletion: C ⁹ →C ⁸ at codon 552	-	-
Δ flgPQ-1	deletion of C-terminal 26 codons of 0661 to codon 61 of downstream gene (<i>dprA</i>)	<i>pglJ</i> : frameshift insertion: A ² →A ³ at codon 287	-	<i>Cji_81176_1435</i> (CPS MeOPN transferase): frameshift deletion: C ⁹ →C ⁸ On→Off; <i>Cji_81176_1341</i> (<i>maf6</i> , putative sugar transferase): frameshift deletion: C ⁹ →C ⁸ On→Off	transition: CGT→TGT at codon 308 (R308C)	-
Δ flgPQ-2 (EJC96)	frameshift deletion: A ⁸ →A ⁷ at codon 322	<i>pglE</i> : frameshift deletion: T ⁹ →T ⁷ at codon 120	<i>kpsD</i> : duplication of codons 147–157	<i>Cji_81176_1420</i> (CPS MeOPN transferase): frameshift deletion: C ⁹ →C ⁸ On→Off; <i>Cji_81176_1428</i> : frameshift deletion: C ¹⁰ →C ⁹ Off→On	transition: GGT→AGT at codon 305 (G305S)	deletion: <i>flaB</i> replaces <i>flaA</i> , <i>flaA</i> promoter drives <i>flaB</i> expression; transition (<i>flaB</i>): ACT→ATT at codon 477 (T477I)

See also Table S1.

directional reversals for chemotaxis occur when motor rotation switches transiently to clockwise, leading to switching which filament is wrapped around the cell body.⁵ This requires that the wrapped filament is pulled free from the cell body via reversal of motor rotation, although the biomechanics of how this causes the filament to be wrenched from the cell surface remains mysterious. What was unexpected in our previous study was the finding that a straight-cell-body mutant struggles to unwrap its wrapped filament. There, we hypothesized that the glycosylated filament and glycosylated cell surface have an affinity for one another and that helical cell shape minimizes contact between the filament and cell surface.

In this study, we find further support for this hypothesis. Selection for suppression of motility defects in Δ flgPQ mutants invariably returned mutations in cell-surface glycosylation genes, while rare flagellar-specific mutations are neither required nor sufficient to promote swimming in the complete absence of a basal disk. Furthermore, the swimming defects of small-disk and displaced-disk mutants are not due to impairment of motor function, as both possess motors that rotate comparably to WT motors.

Inevitably, our results have limitations and unresolved complexities. One of the principal complications is that our suppression experiments returned a combination of mutations affecting different types of surface-sugar interactions: filament-filament interactions involved in autoagglutination and filament-cell body interactions involved in unwrapping during directional switching. Curiously, the suppressors of different types of mutant differ: disk displacement (in the *flgP-lpp*⁵⁶ mutant) is suppressed by reducing filament O-glycosylation, whereas disk removal (by deleting *flgPQ*) is suppressed by abolishing cell-surface glycosylation (by preventing capsule biosynthesis and N-linked glycosylation). Introduction of the *pseG*^{142T} allele into the EJC103 background has no noticeable effect on motility in soft agar (not shown). Similarly, a *flgP-lpp*⁵⁵ Δ *pglAB::aphA* Δ *kpsD* Δ 0661 mutant swims no better than *flgP-lpp*⁵⁵ alone (Figure S4B).

Why do we only see cell-surface glycosylation suppressors and not filament glycosylation suppressors of disk-less mutants? We speculate that the *pseG*^{142T} allele fails to further boost motility in the EJC103 background (the Δ flgPQ mutant lacking CPS, N-glycosylation [i.e., *pgl*], and enigmatic protein 0661) mutant because the *pseG*^{142T} strain's filament is still heavily glycosylated, and a low-torque (due to low stator occupancy) Δ flgPQ motor cannot overcome the still-strong affinity between two glycosylated filaments. That the difference in autoagglutination profiles between WT and *pseG*^{142T} are only apparent following extended incubation periods suggests that the effect of the *pseG*^{142T} allele on filament glycosylation is small and that the un-flanged but otherwise-functional motor in *flgP-lpp*⁵⁵ background is sufficiently powerful to overcome filament-filament adhesion.

Similarly, we found that deletion of surface glycosylation genes (i.e., *pglAB* and *kpsD*) in the *flgP-lpp*⁵⁵ background does not suppress its motility defect in soft agar. Why is this the case? Our results suggest that the defects in soft-agar motility in the Δ flgPQ background and *flgP-lpp*⁵⁵ background are fundamentally different. The motility defect in a disk-less mutant (i.e., Δ flgPQ) is due not only to inefficient stator incorporation into

the motor but also to enhanced autoagglutination. Loss of cell-surface sugars, therefore, allows $\Delta flgPQ$ cells to escape or avoid cell aggregates and remain free swimming. In contrast, the $flgP-lpp^{55}$ defect appears to be almost entirely due to its unwrapping defect, as it has only a moderate autoagglutination defect. Thus, mutations that allow disk-less cells to avoid cell clumps are not expected to alleviate the motility defect of the $flgP-lpp^{55}$ mutant.

Although none of our suppressor screens returned alleles in lipooligosaccharide (LOS) genes, we found that insertional inactivation of *waaF*, involved in LOS biosynthesis, resulted in a slight increase in swarm diameter in the $flgP-lpp^{55}$ background and may potentiate further suppression. Conversely, knockout of CPS in either a WT or $flgP-lpp^{55}$ background significantly reduces soft-agar motility. These results suggest that the filament-cell-surface interaction is complex and may involve multiple interacting partners.

The role of *0661*, deletion of which is required to suppress the $\Delta flgPQ$ motility defect, remains unclear. The gene product of *0661* is a member of the PF04748 divergent polysaccharide deacetylase family and is ubiquitous across Campylobacterota but is absent from other genera (Figure S4C). All Campylobacterota *0661* homologs form a discrete clade within the PF04748 phylogeny, indicating that they retain a common function. Curiously, PF04748 occurs even in the absence of capsule or flagellin glycosylation genes, suggesting an alternative role. The ubiquity of *0661* in the Campylobacterota indicates that this gene is ancient and arose shortly after the Campylobacterota genus branched off from other bacterial taxa. Although we observed no impact of deleting *0661* on growth and motility in an otherwise WT background in a laboratory setting, *0661* is essential for colonization of the chicken cecum.³⁷

We speculate that *0661* may process peptidoglycan based on three observations. First, *0661* is predicted to be an inner-membrane-anchored periplasmic protein, similar to another peptidoglycan acetyltransferase, PatB, in *C. jejuni*³⁸; second, deletion of *0661* has no effect on autoagglutination rate in the $\Delta flgPQ$ background; and third, deletion of *0661* in the $\Delta flgPQ$ mutant results in a transition from ~5% of cells rotating their flagella to ~25% of cells having rotating filaments (not shown), while there is no apparent further increase as *pglAB* and *kpsD* are knocked out, suggesting deletion of *0661* somehow enhances the ability of stators to associate with the motor in the absence of scaffolding. In the model organisms, stator complex protein MotB is believed to bind peptidoglycan via a catch-bond mechanism and has been shown to co-crystallize with *N*-acetylmuramic acid, a component of peptidoglycan.³⁹ Future work will focus on *0661*'s enzymatic activity and whether it defaces a binding motif on peptidoglycan required for efficient recruitment of *Campylobacterota* MotB to the motor.

Investigation of the cell-surface glycome of *C. jejuni* has been an area of intense research for several decades.^{40,41} *N*-linked glycosylation has been shown to be important for protein folding, protection of proteins from proteolytic degradation, natural transformation, and adhesion to host cells^{42–46}; CPS is known to protect against insult by antimicrobials and bacteriophages in the environment, to help modulate and evade the host immune system, and is involved in biofilm formation and host colonization^{34,47,48}; and *O*-glycosylation of the flagellar filament, in addition to promoting filament assembly and autoagglutination, is

known to modulate adhesion to host epithelial cells.^{49,50} Overall, *C. jejuni* devotes a relatively large proportion of its genome (>8%) to genes involved in the decoration of the cell surface with polysaccharides.⁴¹ As *C. jejuni* has evolved an ever-more complex and abundant collection of surface-exposed sugars that it uses to thrive in its environmental niche, it has become, in a word, sticky.

We posit that *C. jejuni* has glycosylated itself into an evolutionary corner: the once-dispensable basal disk and associated stator scaffolding have become indispensable for effective motility as the cell has become more and more sticky. The structural complexity of the *C. jejuni* motor, however, can be reduced to that of a *Salmonella*-type flagellar motor and promote swimming, provided simultaneous devolution of cell-surface glycosylation occurs. In addition to allowing free swimming and unwrapping by individual planktonic cells, we speculate that a flanged motor is important for the dispersal of individual cells from a sessile biofilm glued together by filaments, exopolysaccharide, and eDNA as cells seek out new sites for colonization in their environment.^{51,52}

A major outstanding question to be addressed is the mechanism by which the disk stabilizes the motor to enable it to overcome the attractive forces between filaments and cells. We speculate that this process is a complicated interaction of hook mechanics, OM fluidity, and cell precession. Flagellar wrapping is a common style of swimming for polar flagellates.⁶ In addition to *C. jejuni*, filament wrapping has been observed in *Shewanella putrefaciens*,⁵³ *Helicobacter suis*,³ *Burkholderia* spp., and *Vibrio fischeri*.⁵⁴ Those whose flagellar motors have been imaged all have periplasmic disks. Our findings suggest a common role for the diverse and convergently evolved periplasmic disks seen in polar flagellates.

Limitations of the study

Our study lacks an assay to understand how the disk buttresses the motor at molecular scale. Our results, especially those from the $flgP-lpp^{55}$ mutant and the suppressors of its unwrapping defect, show that the basal disk acts to stabilize and reinforce the motor. Although we presume that this reinforcement arises from flanging of the P-ring, how the basal disk and P-ring interact remains unclear, particularly in light of the ability of the disk to assemble axially out of register with the P-ring. The OM (to which FlgP is anchored), peptidoglycan, or other motor components (e.g., stator scaffolding) may instead contribute to reinforcement of the motor via their interactions with the basal disk. Understanding the mechanical contribution of the disk will ultimately require sophisticated biophysical assays that enable inference of motor orientation, including twist, pitch, and yaw, from observations such as cell precession.

Although our results suggest that a large disk mitigates autoagglutination, the presence of many disk-less and, therefore, paralyzed motors in these backgrounds enables only indirect correlation of disk size with reduced autoagglutination. To determine the extent to which a large disk enables disentangling of interacting filaments will require a mutant in which all cells in the population homogeneously construct small basal disks, a goal made challenging given that each ring of the disk can template a subsequent ring. Control of transcription may therefore be the only practical way to modulate disk diameter.

A further caveat to our findings arises from our inability to determine the direction of motor rotation in our supplemental videos. Because we cannot determine which direction the motor rotates in our videos of the *flgP-lpp*⁵⁵ mutant, it is possible that the unwrapping defect in this background is due to a defect in the chemosensory system, although we find this possibility unlikely.

Lastly, we do not know with which moieties on the cell surface the flagellar filament interacts, although our results suggest that adhesion of the filament to the cell surface involves the O-linked glycans of the filament and polysaccharides on the cell surface. Deciphering these interactions will require a dedicated comprehensive study manipulating various combinations of these systems.

RESOURCE AVAILABILITY

Lead contact

Further information and request for resources and reagents should be directed to and will be fulfilled by the lead contact, Eli J. Cohen (eli.cohen@imperial.ac.uk).

Materials availability

Requests for resources, reagents, and strains should be directed to Eli J. Cohen (eli.cohen@imperial.ac.uk). This study did not generate any new unique reagents.

Data and code availability

- Subtomogram averages have been deposited at the Electron Microscopy Data Bank (www.ebi.ac.uk/emdb) and are publicly available as of the date of publication. EMD accession numbers are listed in the [key resources table](#).
- This paper does not report original code.
- Any additional information required to reanalyze the data reported in this paper is available from the [lead contact](#), Eli J. Cohen (eli.cohen@imperial.ac.uk), upon request.

ACKNOWLEDGMENTS

We thank Paul Simpson in the Imperial College London Electron Microscopy Centre for electron microscopy assistance. This work was supported by Medical Research Council grant MR/V000799/1 to E.J.C. and M.B., NIH grant R01AI065539 to D.R.H., and KAKENHI grant 22H05066 from the Japan Society for the Promotion of Science to D.N. The funders had no role in study design, data collection and analysis, decision to publish, or preparation of the manuscript. J.-J.F. was supported by grant TED2021-132020B-I00 from Spanish MCIN/AEI and NextGenerationEU/PRTR. For the purpose of open access, the author has applied a Creative Commons Attribution (CC BY) license to any Author Accepted Manuscript version arising.

AUTHOR CONTRIBUTIONS

Conceptualization, E.J.C. and M.B.; experimental design and execution, E.J.C. and T.D.; strain construction, E.J.C., T.D., X.G., and D.R.H.; data collection and analysis, E.J.C. and T.D.; preparation of manuscript, E.J.C. and M.B.; chick colonization assays, D.A.R. and D.R.H.; microfluidics microscopy, A.Y.; electron microscopy data collection, E.J.C. and T.U.; data analysis, E.J.C., L.W., T.D. and J.-J.F.; holographic microscopy data collection, E.E.B.; holographic microscopy data analysis, L.W.; fluorescence microscopy data collection and analysis, E.J.C. and D.N.; experimental design, E.J.C. and M.B.

DECLARATION OF INTERESTS

The authors declare no competing interests.

STAR★METHODS

Detailed methods are provided in the online version of this paper and include the following:

- [KEY RESOURCES TABLE](#)
- [EXPERIMENTAL MODEL AND STUDY PARTICIPANT DETAILS](#)
 - Infection of avian hosts
 - Age and development of avian hosts
 - Housing conditions of avian hosts
 - Considerations of sex and gender as a biological variable
 - Authorization of *in vivo* vertebrate usage
- [METHOD DETAILS](#)
 - Cultivation of *C. jejuni*
 - Soft agar motility assays
 - Genetic manipulation of *C. jejuni*
 - Western blotting
 - Filament depolymerization for blotting
 - Autoagglutination assays
 - 3D-holographic microscopy
 - High-speed fluorescence microscopy
 - Aerotaxis assays
 - Microfluidic experiments
 - Negative stain TEM
 - Chicken colonization assays
- [QUANTIFICATION AND STATISTICAL ANALYSIS](#)

SUPPLEMENTAL INFORMATION

Supplemental information can be found online at <https://doi.org/10.1016/j.devcel.2024.09.008>.

Received: January 7, 2024

Revised: June 10, 2024

Accepted: September 9, 2024

Published: October 2, 2024

REFERENCES

1. Beeby, M., Ferreira, J.L., Tripp, P., Albers, S.-V., and Mitchell, D.R. (2020). Propulsive nanomachines: the convergent evolution of archaella, flagella and cilia. *FEMS Microbiol. Rev.* **44**, 253–304.
2. Ferreira, J.L., Coleman, I., Addison, M.L., Zachs, T., Quigley, B.L., Wuichet, K., and Beeby, M. (2021). The ‘jack-of-all-trades’ flagellum from *Salmonella* and *E. coli* Was horizontally acquired from an ancestral β -proteobacterium. *Front. Microbiol.* **12**, 643180.
3. Constantino, M.A., Jabbarzadeh, M., Fu, H.C., Shen, Z., Fox, J.G., Haesebrouck, F., Linden, S.K., and Bansil, R. (2018). Bipolar lophotrichous *Helicobacter suis* combine extended and wrapped flagella bundles to exhibit multiple modes of motility. *Sci. Rep.* **8**, 14415.
4. Murat, D., Hérissé, M., Espinosa, L., Bossa, A., Alberto, F., and Wu, L.F. (2015). Opposite and coordinated rotation of amphitrichous flagella governs oriented swimming and reversals in a magnetotactic *Spirillum*. *J. Bacteriol.* **197**, 3275–3282.
5. Cohen, E.J., Nakane, D., Kabata, Y., Hendrixson, D.R., Nishizaka, T., and Beeby, M. (2020). *Campylobacter jejuni* motility integrates specialized cell shape, flagellar filament, and motor, to coordinate action of its opposed flagella. *PLoS Pathog.* **16**, e1008620.
6. Thormann, K.M., Beta, C., and Kühn, M.J. (2022). Wrapped up: the motility of polarly flagellated bacteria. *Annu. Rev. Microbiol.* **76**, 349–367.
7. Waite, D.W., Chuvpochina, M.S., and Hugenholtz, P. (2019). Road map of the phylum *Campylobacterota*. In *Bergey’s Manual of Systematics of Archaea and Bacteria 1–11* (John Wiley & Sons, Ltd). <https://doi.org/10.1002/9781118960608.bm00040>.
8. Beeby, M., Ribardo, D.A., Brennan, C.A., Ruby, E.G., Jensen, G.J., and Hendrixson, D.R. (2016). Diverse high-torque bacterial flagellar motors

- assemble wider stator rings using a conserved protein scaffold. *Proc. Natl. Acad. Sci. USA* **113**, E1917–E1926.
9. Drobnič, T., Cohen, E.J., Alzheimer, M., Froschauer, K., Svensson, S., Singh, N., Garg, S.G., Henderson, L., Umrekar, T., Nans, A., et al. (2023). Molecular model of a bacterial flagellar motor *in situ* reveals a “parts-list” of protein adaptations to increase torque. Preprint at bioRxiv. <https://doi.org/10.1101/2023.09.08.556779>.
 10. Cohen, E.J., Quek, R.T., and Beeby, M. (2019). A tetRA-based promoter system for the generation of conditional knockouts in *Campylobacter jejuni*. Preprint at bioRxiv. <https://doi.org/10.1101/616649>.
 11. Misawa, N., and Blaser, M.J. (2000). Detection and characterization of autoagglutination activity by *Campylobacter jejuni*. *Infect. Immun.* **68**, 6168–6175.
 12. Trunk, T., Khalil, H.S., and Leo, J.C. (2018). Bacterial autoaggregation. *AIMS Microbiol.* **4**, 140–164.
 13. Cohen, E.J., Ferreira, J.L., Ladinsky, M.S., Beeby, M., and Hughes, K.T. (2017). Nanoscale-length control of the flagellar driveshaft requires hitting the tethered outer membrane. *Science* **356**, 197–200.
 14. Asmar, A.T., Ferreira, J.L., Cohen, E.J., Cho, S.H., Beeby, M., Hughes, K.T., and Collet, J.F. (2017). Communication across the bacterial cell envelope depends on the size of the periplasm. *PLoS Biol.* **15**, e2004303.
 15. Mathelié-Guinlet, M., Asmar, A.T., Collet, J.-F., and Dufrene, Y.F. (2020). Lipoprotein Lpp regulates the mechanical properties of the *E. coli* cell envelope. *Nat. Commun.* **11**, 1789.
 16. Chevance, F.F.V., Takahashi, N., Karlinsey, J.E., Gnerer, J., Hirano, T., Samudrala, R., Aizawa, S.I., and Hughes, K.T. (2007). The mechanism of outer membrane penetration by the eubacterial flagellum and implications for spirochete evolution. *Genes Dev.* **21**, 2326–2335. <https://doi.org/10.1101/gad.1571607>.
 17. Moriya, N., Minamino, T., Ferris, H.U., Morimoto, Y.V., Ashihara, M., Kato, T., and Namba, K. (2013). Role of the Dc domain of the bacterial hook protein FlgE in hook assembly and function. *Biophys J.* **9**, 63–72.
 18. Matsunami, H., Barker, C.S., Yoon, Y.-H., Wolf, M., and Samatey, F.A. (2016). Complete structure of the bacterial flagellar hook reveals extensive set of stabilizing interactions. *Nat. Commun.* **7**, 13425.
 19. Horváth, P., Kato, T., Miyata, T., and Namba, K. (2019). Structure of salmonella flagellar hook reveals intermolecular domain interactions for the universal joint function. *Biomolecules* **9**, 462.
 20. Liu, F., and Tanner, M.E. (2006). PseG of pseudaminic acid biosynthesis: a UDP-sugar hydrolase as a masked glycosyltransferase. *J. Biol. Chem.* **281**, 20902–20909.
 21. Rangarajan, E.S., Proteau, A., Cui, Q., Logan, S.M., Potetinova, Z., Whitfield, D., Purisima, E.O., Cygler, M., Matte, A., Sulea, T., et al. (2009). Structural and Functional Analysis of *Campylobacter jejuni* PseG: a UDP-sugar hydrolase from the Pseudaminic Acid Biosynthetic pathway. *J. Biol. Chem.* **284**, 20989–21000.
 22. Ewing, C.P., Andreishcheva, E., and Guerry, P. (2009). Functional characterization of flagellin glycosylation in *Campylobacter jejuni* 81–176. *J. Bacteriol.* **191**, 7086–7093.
 23. Doig, P., Kinsella, N., Guerry, P., and Trust, T.J. (1996). Characterization of a post-translational modification of *Campylobacter flagellin*: identification of a sero-specific glycosyl moiety. *Mol. Microbiol.* **19**, 379–387.
 24. Thibault, P., Logan, S.M., Kelly, J.F., Brisson, J.R., Ewing, C.P., Trust, T.J., and Guerry, P. (2001). Identification of the carbohydrate moieties and glycosylation motifs in *Campylobacter jejuni* flagellin. *J. Biol. Chem.* **276**, 34862–34870.
 25. McNally, D.J., Hui, J.P.M., Aubry, A.J., Mui, K.K.K., Guerry, P., Brisson, J.R., Logan, S.M., and Soo, E.C. (2006). Functional characterization of the flagellar glycosylation locus in *Campylobacter jejuni* 81–176 using a focused metabolomics approach. *J. Biol. Chem.* **281**, 18489–18498.
 26. Guerry, P., Ewing, C.P., Schirm, M., Lorenzo, M., Kelly, J., Pattarini, D., Majam, G., Thibault, P., and Logan, S. (2006). Changes in flagellin glycosylation affect *Campylobacter* autoagglutination and virulence. *Mol. Microbiol.* **60**, 299–311.
 27. Karlyshev, A.V., Linton, D., Gregson, N.A., Lastovica, A.J., and Wren, B.W. (2000). Genetic and biochemical evidence of a *Campylobacter jejuni* capsular polysaccharide that accounts for Penner serotype specificity. *Mol. Microbiol.* **35**, 529–541.
 28. Oldfield, N.J., Moran, A.P., Millar, L.A., Prendergast, M.M., and Ketley, J.M. (2002). Characterization of the *Campylobacter jejuni* heptosyltransferase II gene, waaf, provides genetic evidence that extracellular polysaccharide is lipid A core independent. *J. Bacteriol.* **184**, 2100–2107.
 29. Cohen, E.J., and Hughes, K.T. (2014). Rod-to-hook transition for extracellular flagellum assembly is catalyzed by the L-ring-dependent rod scaffold removal. *J. Bacteriol.* **196**, 2387–2395.
 30. Szymanski, C.M., Yao, R., Ewing, C.P., Trust, T.J., and Guerry, P. (1999). Evidence for a system of general protein glycosylation in *Campylobacter jejuni*. *Mol. Microbiol.* **32**, 1022–1030.
 31. Kelly, J., Jarrell, H., Millar, L., Tessier, L., Fiori, L.M., Lau, P.C., Allan, B., and Szymanski, C.M. (2006). Biosynthesis of the N-linked glycan in *Campylobacter jejuni* and addition onto protein through block transfer. *J. Bacteriol.* **188**, 2427–2434.
 32. Cain, J.A., Dale, A.L., Sumer-Bayraktar, Z., Solis, N., and Cordwell, S.J. (2020). Identifying the targets and functions of N-linked protein glycosylation in *Campylobacter jejuni*. *Mol. Omics* **16**, 287–304.
 33. Scott, N.E., Parker, B.L., Connolly, A.M., Paulech, J., Edwards, A.V.G., Crossett, B., Falconer, L., Kolarich, D., Djordjevic, S.P., Højrup, P., et al. (2011). Simultaneous glycan-peptide characterization using hydrophilic interaction chromatography and parallel fragmentation by CID, higher energy collisional dissociation, and electron transfer dissociation MS applied to the N-linked glycoproteome of *Campylobacter jejuni*. *Mol. Cell. Proteomics* **10**, M000031-MMCP201.
 34. Bacon, D.J., Szymanski, C.M., Burr, D.H., Silver, R.P., Alm, R.A., and Guerry, P. (2001). A phase-variable capsule is involved in virulence of *Campylobacter jejuni* 81–176. *Mol. Microbiol.* **40**, 769–777.
 35. van Alphen, L.B., Wenzel, C.Q., Richards, M.R., Fodor, C., Ashmus, R.A., Stahl, M., Karlyshev, A.V., Wren, B.W., Stintzi, A., Miller, W.G., et al. (2014). Biological roles of the O-methyl phosphoramidate capsule modification in *Campylobacter jejuni*. *PLoS One* **9**, e87051.
 36. Paul, K., Gonzalez-Bonet, G., Bilwes, A.M., Crane, B.R., and Blair, D. (2011). Architecture of the flagellar rotor. *EMBO J.* **30**, 2962–2971.
 37. Johnson, J.G., Livny, J., and DiRita, V.J. (2014). High-throughput sequencing of *Campylobacter jejuni* insertion mutant libraries reveals mapA as a fitness factor for chicken colonization. *J. Bacteriol.* **196**, 1958–1967.
 38. Iwata, T., Watanabe, A., Kusumoto, M., and Akiba, M. (2016). Peptidoglycan acetylation of *Campylobacter jejuni* is essential for maintaining cell wall integrity and colonization in chicken intestines. *Appl. Environ. Microbiol.* **82**, 6284–6290.
 39. Roujeinikova, A. (2008). Crystal structure of the cell wall anchor domain of MotB, a stator component of the bacterial flagellar motor: implications for peptidoglycan recognition. *Proc. Natl. Acad. Sci. USA* **105**, 10348–10353.
 40. Szymanski, C.M., Logan, S.M., Linton, D., and Wren, B.W. (2003). *Campylobacter* – a tale of two protein glycosylation systems. *Trends Microbiol.* **11**, 233–238.
 41. Karlyshev, A.V., Ketley, J.M., and Wren, B.W. (2005). The *Campylobacter jejuni* glycome. *FEMS Microbiol. Rev.* **29**, 377–390.
 42. Cain, J.A., Dale, A.L., Niewold, P., Klare, W.P., Man, L., White, M.Y., Scott, N.E., and Cordwell, S.J. (2019). Proteomics reveals multiple phenotypes associated with N-linked glycosylation in *Campylobacter jejuni*. *Mol. Cell. Proteomics* **18**, 715–734.
 43. Duma, J., Nothaft, H., Weaver, D., Fodor, C., Beadle, B., Linton, D., Benoit, S.L., Scott, N.E., Maier, R.J., and Szymanski, C.M. (2020). Influence of protein glycosylation on *Campylobacter fetus* physiology. *Front. Microbiol.* **11**, 1191.
 44. Alemka, A., Nothaft, H., Zheng, J., and Szymanski, C.M. (2013). N-glycosylation of *Campylobacter jejuni* Surface proteins promotes bacterial fitness. *Infect. Immun.* **81**, 1674–1682.

45. Abouelhadid, S., Raynes, J., Bui, T., Cuccui, J., and Wren, B.W. (2020). Characterization of posttranslationally modified multidrug efflux pumps reveals an unexpected link between glycosylation and antimicrobial resistance. *mBio* *11*, e02604–e02620.
46. Abouelhadid, S., North, S.J., Hitchen, P., Vohra, P., Chintoan-Uta, C., Stevens, M., Dell, A., Cuccui, J., and Wren, B.W. (2019). Quantitative analyses reveal novel roles for N-glycosylation in a major enteric bacterial pathogen. *mBio* *10*, e00297-19.
47. Maue, A.C., Mohawk, K.L., Giles, D.K., Poly, F., Ewing, C.P., Jiao, Y., Lee, G., Ma, Z., Monteiro, M.A., Hill, C.L., et al. (2013). The polysaccharide capsule of *Campylobacter jejuni* modulates the host immune response. *Infect. Immun.* *81*, 665–672.
48. Coward, C., Grant, A.J., Swift, C., Philp, J., Towler, R., Heydarian, M., Frost, J.A., and Maskell, D.J. (2006). Phase-variable surface structures are required for infection of *Campylobacter jejuni* by bacteriophages. *Appl. Environ. Microbiol.* *72*, 4638–4647.
49. Guerry, P. (2007). *Campylobacter* flagella: not just for motility. *Trends Microbiol.* *15*, 456–461.
50. Merino, S., and Tomás, J.M. (2014). Gram-negative flagella glycosylation. *Int. J. Mol. Sci.* *15*, 2840–2857.
51. Tram, G., Day, C.J., and Korolik, V. (2020). Bridging the gap: A role for *Campylobacter jejuni* biofilms. *Microorganisms* *8*, 452.
52. Howard, S.L., Jagannathan, A., Soo, E.C., Hui, J.P.M., Aubry, A.J., Ahmed, I., Karlyshev, A., Kelly, J.F., Jones, M.A., Stevens, M.P., et al. (2009). *Campylobacter jejuni* glycosylation island important in cell charge, legionaminic acid biosynthesis, and colonization of chickens. *Infect. Immun.* *77*, 2544–2556.
53. Kühn, M.J., Schmidt, F.K., Eckhardt, B., and Thormann, K.M. (2017). Bacteria exploit a polymorphic instability of the flagellar filament to escape from traps. *Proc. Natl. Acad. Sci. USA* *114*, 6340–6345.
54. Kinoshita, Y., Kikuchi, Y., Mikami, N., Nakane, D., and Nishizaka, T. (2018). Unforeseen swimming and gliding mode of an insect gut symbiont, *Burkholderia* sp. RPE64, with wrapping of the flagella around its cell body. *ISME J.* *12*, 838–848.
55. Hendrixson, D.R., Akerley, B.J., and DiRita, V.J. (2001). Transposon mutagenesis of *Campylobacter jejuni* identifies a bipartite energy taxis system required for motility. *Mol. Microbiol.* *40*, 214–224.
56. Beauchamp, J.M., Leveque, R.M., Dawid, S., and DiRita, V.J. (2017). Methylation-dependent DNA discrimination in natural transformation of *Campylobacter jejuni*. *Proc. Natl. Acad. Sci. USA* *114*, E8053–E8061.
57. Wilson, L., and Zhang, R. (2012). 3D Localization of weak scatterers in digital holographic microscopy using Rayleigh-Sommerfeld back-propagation. *Opt. Express* *20*, 16735–16744.
58. Kühn, M.J., Schmidt, F.K., Farthing, N.E., Rossmann, F.M., Helm, B., Wilson, L.G., Eckhardt, B., and Thormann, K.M. (2018). Spatial arrangement of several flagellins within bacterial flagella improves motility in different environments. *Nat. Commun.* *9*, 5369.
59. Thornton, K.L., Butler, J.K., Davis, S.J., Baxter, B.K., and Wilson, L.G. (2020). Haloarchaea swim slowly for optimal chemotactic efficiency in low nutrient environments. *Nat. Commun.* *11*, 4453.
60. Weibel, D.B., DiLuzio, W.R., and Whitesides, G.M. (2007). Microfabrication meets microbiology. *Nat. Rev. Microbiol.* *5*, 209–218.
61. Agulleiro, J.I., and Fernandez, J.J. (2011). Fast tomographic reconstruction on multicore computers. *Bioinform. Oxf. Engl.* *27*, 582–583.
62. Agulleiro, J.-I., and Fernandez, J.-J. (2015). Tomo3D 2.0—exploitation of advanced vector extensions (AVX) for 3D reconstruction. *J. Struct. Biol.* *189*, 147–152.
63. Tegunov, D., and Cramer, P. (2019). Real-time cryo-electron microscopy data preprocessing with Warp. *Nat. Methods* *16*, 1146–1152.
64. Schindelin, J., Arganda-Carreras, I., Frise, E., Kaynig, V., Longair, M., Pietzsch, T., Preibisch, S., Rueden, C., Saalfeld, S., Schmid, B., et al. (2012). Fiji: an open-source platform for biological-image analysis. *Nat. Methods* *9*, 676–682.
65. Suloway, C., Pulokas, J., Fellmann, D., Cheng, A., Guerra, F., Quispe, J., Stagg, S., Potter, C.S., and Carragher, B. (2005). Automated molecular microscopy: the new Leginon system. *J. Struct. Biol.* *151*, 41–60.
66. Cheng, A., Negro, C., Bruhn, J.F., Rice, W.J., Dallakyan, S., Eng, E.T., Waterman, D.G., Potter, C.S., and Carragher, B. (2021). Leginon: new features and applications. *Protein Sci.* *30*, 136–150.
67. Castaño-Díez, D., Kudryashev, M., Arheit, M., and Stahlberg, H. (2012). Dynamo: A flexible, user-friendly development tool for subtomogram averaging of cryo-EM data in high-performance computing environments. *J. Struct. Biol.* *178*, 139–151.
68. Kremer, J.R., Mastronarde, D.N., and McIntosh, J.R. (1996). Computer visualization of three-dimensional image data using IMOD. *J. Struct. Biol.* *116*, 71–76.

STAR★METHODS

KEY RESOURCES TABLE

REAGENT or RESOURCE	SOURCE	IDENTIFIER
Antibodies		
Rabbit polyclonal anti-FlgP antisera	Laboratory of David R. Hendrixson	N/A
Rabbit polyclonal anti-FlgR	Laboratory of David R. Hendrixson	N/A
Goat anti-rabbit HRP-conjugated antibody	Enzo Life Sciences	Cat#ADI-SAB-300-J
Bacterial and virus strains		
See Table 1 in the main text for a list of bacterial strains used in this study.	This paper	N/A
Chemicals, peptides, and recombinant proteins		
Q5 DNA polymerase	New England Biolabs	Cat#M0491L
EcoRI methyltransferase	New England Biolabs	Cat#M0211S
FM 4-64 dye	Thermo Fisher Scientific/Invitrogen	Cat#T13320
DyLight 488 maleimide dye	Thermo Scientific	Cat#46602
Anhydrotetracycline HCl	Sigma-Aldrich	Cat#37919
Methylcellulose 4000 cP	Sigma-Aldrich	Cat#M0512
Critical commercial assays		
Clarity Western ECL Substrate	Bio-Rad Laboratories Ltd.	Cat#1705061
Novex pH 3-7 IEF Protein Gels, 1.0 mm, 10-well	Thermo Fisher Scientific/Invitrogen	Cat#EC6645BOX
Deposited data		
Subtomogram average of EJC168 12.5 ng/mL ATc	This paper	Electron Microscopy Database: EMD-17769
Subtomogram average of EJC168 25 ng/mL ATc	This paper	Electron Microscopy Database: EMD-17770
Subtomogram average of EJC168 50 ng/mL ATc	This paper	Electron Microscopy Database: EMD-17771
Subtomogram average of EJC168 100 ng/mL ATc	This paper	Electron Microscopy Database: EMD-17772
Subtomogram average of <i>flgP</i> ^{AAA}	This paper	Electron Microscopy Database: EMD-17773
Subtomogram average of <i>flgP</i> ^{Δ18-62}	This paper	Electron Microscopy Database: EMD-17774
Subtomogram average of <i>flgP-lpp</i> ⁵⁵	This paper	Electron Microscopy Database: EMD-18274
Subtomogram average of <i>ΔflgPQ</i>	This paper	Electron Microscopy Database: EMD-17775
Subtomogram average of <i>ΔflgPQ</i> <i>Δ0661 ΔkpsD ΔpglAB::aphA</i>	This paper	Electron Microscopy Database: EMD-17776
Experimental models: Organisms/strains		
Fertilized eggs from White Leghorn chickens	Charles River SPAFAS	N/A
Oligonucleotides		
See Table S1 for a list of oligonucleotides used for strain construction in this study.	Integrated DNA Technologies (IDT)	N/A
Software and algorithms		
ImageJ/FIJI v2.1.0/1.53c	Schindelin et al. ⁶⁴	N/A
Leginon 3.6	Suloway et al. ⁶⁵ ; Cheng et al. ⁶⁶	N/A
Dynamo 1.1.532	Castaño-Díez et al. ⁶⁷	N/A
IMOD 4.11	Kremer et al. ⁶⁸	N/A
Geneious Prime 2021.0.3	Biomatters, New Zealand	N/A
Tomo3D 2	Agulleiro and Fernandez ^{61,62}	N/A

EXPERIMENTAL MODEL AND STUDY PARTICIPANT DETAILS

Infection of avian hosts

Specific pathogen-free fertilized eggs from white leghorn chickens were procured from Charles River SPAFAS. White leghorn chickens are an outbred strain.

Age and development of avian hosts

Fertilized eggs from white leghorn chickens were incubated for 21 days at 37.5 °C for 21 d with appropriate humidity and rotation in a Digital Sportsman model 1502 incubator (Georgia Quail Farms). All subsequent infections with *Campylobacter jejuni* only involved chickens within 24 h of hatch. Undeveloped chicks in eggs were not used in any infection.

Housing conditions of avian hosts

Within 24 h of hatch, groups of at least six chicks were placed into brooders and given water and generic chick feed ad libitum. Heat was provided with a heat lamp. Due to these conditions, the chickens developed a normal gastrointestinal flora.

Considerations of sex and gender as a biological variable

As chicks upon hatching are difficult to sex type, both male and female chicks were included in all studies and randomly assigned to control and experimental groups. There is no known association of sex and gender of outbred white leghorn chickens with colonization by *Campylobacter jejuni*.

Authorization of *in vivo* vertebrate usage

All use of animals in experimentation has been approved by IACUC at the University of Texas Southwestern Medical Center.

METHOD DETAILS

Cultivation of *C. jejuni*

All strains of *C. jejuni* used in this study are derivatives of DRH212 (*rpsL*^{K88R}), a streptomycin-resistant isolate of *C. jejuni* strain 81-176.⁵⁵ For all experiments, cultures were grown at 37°C on 1.4% Mueller-Hinton agar supplemented with 10 µg/mL Trimethoprim (MHT agar) plus other antibiotics as needed. Soft agar for motility assays used 0.35% MHT agar. Antibiotics were added as needed at the following concentrations: kanamycin, 50 µg/mL; chloramphenicol, 12.5 µg/mL; Streptomycin, 200 µg/mL and 2 mg/mL; Anhydrotetracycline HCl, 0.0125–0.2 µg/mL.

For experiments at Imperial College London and UT Southwestern, cultures were grown microaerobically (85% N₂, 10% CO₂, 5% O₂) in trigas incubators. Thermo-Fisher Campygen (University of York) and Mitsubishi (UEC) Gas-generating sachets were used at University of York and University of Electrocommunications, respectively.

Cell suspensions for optical microscopy experiments, tomography, and autoagglutination assays were prepared by seeding a small amount of culture from a -80°C master stock on a fresh MHT plate. Following 20–24 hours incubation, overnight growth of the inoculum was spread on another fresh MHT plate and incubated overnight. In the morning, fresh growth was gently washed off the plate into MH broth by pipetting.

Soft agar motility assays

For soft agar motility assays, a small amount of fresh overnight growth from an MHT plate was poked into 0.4% agar MHT using a toothpick and incubated microaerobically for 18–48 hours. All swarm assays were performed in triplicate.

For each of the four lineages in the $\Delta flgQ/\Delta flgPQ$ evolution experiment, a single colony at day 0 was poked into 0.4% agar MHT and incubated microaerobically for 4–5 days, at which point the periphery or any flares from the initial point of inoculation were picked with a toothpick and poked a single time into a fresh 0.4% agar MHT plate. This was repeated 4–5 times, at which point all four of the lineages had evolved from a non-motile phenotype to a non-bushy mot+ phenotype. As our trigas incubator maintains ~100% humidity at all times, evaporation from the agar during the extended incubation periods of the evolution experiment was presumed to be negligible.

Genetic manipulation of *C. jejuni*

All mutations generated in this study are chromosomally integrated at their native loci, unless otherwise stated. In-frame markerless gene deletions were constructed by leaving several N- and C-terminal residues of the targeted gene intact in order to minimize polarity on flanking genes. For the $\Delta kpsD$ allele, the deletion covers from I24 to V520. For the *Cjj_81176_0661* clean deletion, residues F19 to K322 were removed. For the $\Delta flgPQ$ strain, the deletion covered from codon 17 of *flgP* codon 129 of *flgQ*, and the $\Delta flgQ$ deletion spanned from codon 56 to 129 of *flgQ*. The *pglAB::aphA* replaces codon 24 of *pglB* to codon 360 of *pglA* with *aphA*, conferring kanamycin resistance.

Strain construction was performed as previously described. Briefly, an *aphA-rpsL*^{WT} cassette with 500–1000 bp of flanking homology to the targeted gene was introduced by natural transformation, selecting for kanamycin resistance (Km^R) and screening for streptomycin sensitivity (Sm^S) on 200 µg/mL streptomycin (the *rpsL*^{WT} allele is dominant to *rpsL*^{K88R} in the merodiploid). Counterselection for loss of the *aphA-rpsL*^{WT} cassette was accomplished by transformation of the Km^R Sm^S intermediate strain with a fragment of DNA encoding the desired mutation, selecting for Sm^R on 2 mg/mL streptomycin and screening for Km^S. Sm^R Km^S transformants were single colony purified, sequenced and stored at -80°C.

For all transformations, linear DNA was generated by SOE PCR as described previously. *ecoRI* sites were added to both ends of each fragment for methylation in order to increase transformation efficiency.⁵⁶ Typically 1–2 µg of methylated DNA was transformed for the initial Km^R selection, and 5–10 µg for the Sm^S counterselection.

Western blotting

Western blotting was performed using whole-cell lysates. Cells were washed off plates into MH broth and the O.D.₆₀₀ adjusted to 0.5 prior to boiling in 2x SDS Laemmli buffer. 15 μ L of each sample was run on either 12% or 4-20% Novex wedgewell tris-glycine polyacrylamide gels. Separated proteins were transferred to 0.2 μ m nitrocellulose membrane using an iBlot 2 transfer apparatus. Secondary antibodies were HRP-conjugated and imaging was performed using Clarity Western ECL substrate (Bio-rad) and a Chemidoc imaging system (Bio-rad)

Western blotting for FlgP was performed using anti-FlgP antisera raised in rabbit. Western blotting for the 6xHis-tag was performed using either HRP-conjugated primary antibody (Sigma, rabbit) or non-HRP-conjugated antisera (rabbit). Western blotting for FlgR was performed using anti-FlgR antisera raised in rabbit.

Filament depolymerization for blotting

To characterize differences between the flagellar filaments in the flgP-lpp⁵⁵ and flgP-lpp⁵⁵ pseG^{I142T} mutants, overnight cultures of each strain were washed off solid MHT agar to an O.D.₆₀₀ of \sim 1.0. 1 mL of cell suspension was added to 100 mL of MHT broth supplemented with 10 mM MgSO₄·7H₂O and grown microaerobically with shaking to early-mid log phase (O.D.₆₀₀ \sim 0.4). Cells were pelleted and washed 2x with PBS before being suspended in a pH 2.2 solution of 200 mM glycine and incubated with gentle agitation at room temperature for 30 minutes to depolymerize the flagellar filaments. Following depolymerization, the cell suspensions adjusted to pH 7 with 2M NaOH.

Following neutralization, cells were pelleted by centrifuging at 20k x g for 20 minutes. 15 mL of each supernatant were then concentrated \sim 100 fold with a centrifugal filter unit (Amicon Ultra Centrifugal Filter unit, 30kDa MWCO).

For Coomassie blots, concentrated supernatants were mixed 1:1 with 2xSDS loading buffer with 5% β -mercaptoethanol and briefly boiled. 10 μ L of each sample was run on a 12% continuous Tris-Glycine SDS-PAGE gel (Novex Wedgewell) and stained/destained according to manufacturer's recommendations (ProteinArk Quick Coomassie).

For IEF gels, the manufacturer's recommended protocol was followed (ThermoFisher Scientific Novex IEF gels, pH 3-7). One gel was run at 100 V for one hour, followed by 1.5 hours at 200 V. A second, identical gel was run for 1 hour at 100 V, 1 hour at 200 V and 30 minutes at 300 V. Protein bands were fixed via 30 minute incubation in 12% trichloroacetic acid, followed by Coomassie staining (ProteinArk Quick Coomassie)

Autoagglutination assays

For autoagglutination assays, fresh growth was washed from plates to an O.D.₆₀₀ of 1.0 in 90:10 PBS:MH broth. 1 mL of cell suspensions were pipetted into disposable 1.25 cm polystyrene cuvettes and left to sit at ambient temperature (21-23°C) for 24 hours. O.D.₆₀₀ measurements were taken with a benchtop cell density meter (Amersham Biosciences Ultrospec 10) every hour for 6-8 hours, as well as a final reading at 24 hours. For O.D.₆₀₀ reading, samples were not collected from the top portion of the cell suspensions. Rather, measurements were taken directly from the original 1 mL cell suspensions in their cuvettes.

3D-holographic microscopy

Holographic cell tracking was performed on an inverted microscope as previously described.⁵⁷ In brief, sample chambers measuring 20 \times 5 \times 0.3 mm³ were constructed from glass slides and coverslips. These chambers were loaded with cell suspensions diluted to a concentration of approximately 3 \times 10⁶ cells/ml. The standard condenser assembly in the microscope was replaced with a holder for a single-mode optical fibre directed along the optical axis of the microscope. A fibre coupled laser with a wavelength of λ =642 nm and an optical power at the sample of 3 mW/cm² was used to illuminate the sample. The sample was imaged using a 20 \times magnification objective lens onto a camera with pixel size of 14 μ m, leading to a spatial sampling frequency of 1.422 pixels/ μ m. Images were acquired at 100 Hz with a 3 ms exposure time. Background correction was performed by creating an image from the median pixel value at each (x,y) location, then dividing the pixel value in each frame by its corresponding value in the median image. We used Rayleigh-Sommerfeld back-propagation to create a stack of refocused images from each frame of the raw video and segmented the corresponding 2D image stack by finding places in which the axial intensity gradient lay above a certain (manually-determined) threshold. These locations are candidates for cell positions. We then linked the coordinates in subsequent frames into cell tracks,⁵⁸ which were subjected to further analysis. Tracks shorter than 0.4 seconds were discarded. These were typically the result of cells entering and leaving the field of view. We calculated the mean-squared displacement (MSD,) for each cell,⁵⁹ and fitted the first second of data with the function . The exponent indicates the nature of the cell's motion and takes values between 1 (diffusive motion) and 2 (purely straight-line swimming). These values are plotted against the cells' root-mean-squared displacement after 1 second (obtained by extrapolation for short tracks) in [Figure 2](#).

High-speed fluorescence microscopy

High-speed videos were recorded as described previously.⁵ Briefly, specimen chambers were prepared by adhering a 24 mm x 40 mm coverslip to a 18 mm x 18 mm coverslip using porous double-sided tape (Nichiban (size 02)). Following pipetting of sample into specimen chambers, chambers were sealed with clear nail lacquer to reduce drift.

We used DyLight 488-conjugated maleimide dye (Thermo Fisher) to label flagellar filaments. Cell bodies were labelled using FM 4-64 dye (Life Technologies). Labelling was carried out by using PBS to wash cells off MH plates to an O.D.₆₀₀ of \sim 1, washing cells 1x in PBS by pelleting cells at 10,000 x g and resuspension in fresh PBS, to which Dylight 488-conjugated maleimide was added and

incubated at 37°C for 20 minutes before addition of FM 4-64, immediately after which cells were pelleted again and resuspended in fresh MH + 0.5% methylcellulose. Unless otherwise stated, all movies were captured at 400 frames per second, and cell suspensions were MH broth supplemented with methylcellulose (4000 cP, Sigma Aldrich) to a final concentration of 0.5%.

Movies were captured with an inverted microscope (IX83, Olympus), equipped with an objective lens (UPLXAPO100×OPH, N.A. 1.45, Olympus), dichroic mirrors (Di01-R488, Semrock), dual-view imaging system with optical filters (FF560-FDi01, FF03-535/50 and BLP01-568R, Semrock), a CMOS camera (Zyla 4.2, Andor), and an optical table (ASD-1510T, JVI). Projection of the image to the camera was made at 0.065 μm per pixel. The focal position of the sample was kept at the focal position by a Z-drift compensation module (ZDC, Olympus). A blue laser beam (OBIS488-20, Coherent) was introduced into the microscope, and the resultant fluorescent images were acquired by imaging software (Solis, Andor) as 16-bit images under 2.5-ms intervals.

Aerotaxis assays

Aerotaxis assays were performed as described previously.⁵ Briefly, specimen chambers were prepared by adhering a 24 mm x 40 mm coverslip to a 18 mm x 18 mm coverslip using porous double-sided tape (Nichiban (size 02)).

Cell suspensions were adjusted to an O.D.₆₀₀ of ~1 and pipetted into a sample chamber. Due to the speed at which populations of WT cells will aerotax, sample chambers were not sealed with clear nail lacquer. Recording was started prior to the addition of samples for the same reason.

Movies were recorded at 3 frames per second using a darkfield microscope (IX83, Olympus) equipped with an objective lens (CPLFLN10×PH, N.A. 0.3, Olympus), darkfield condenser (U-DCD, Olympus), and a CMOS camera (Zyla 4.2, Andor) and an optical table (ASD-1510T, JVI). Projection of the image to the camera was made at 0.65 μm per pixel. Sequential images of cells were acquired by the imaging software (Solis; Andor) as 16-bit images with the CMOS camera.

Kymographs were generated in ImageJ version 1.48. The height of the sequential images was resized to one pixel and aligned vertically so that the y-axis represents time.

Microfluidic experiments

Microfluidic devices with confined 1 μm channels were fabricated using standard photolithography and soft lithography methods as described previously.⁶⁰ Briefly, polydimethylsiloxane (PDMS, Sylgard 184, Dow), a two-part silicone elastomer, was cast over a photolithography master and cured at room temperature for 48 h. A piece of PDMS was cut out using a scalpel and used as a microfluidic device. Cell suspensions with MH broth containing 0.5% methylcellulose, were dropped onto a glass slide and then covered with the microfluidic device casting from the top. Movies were captured with an inverted microscope (IX73, Olympus), equipped with an objective lens (UPLXAPO100×OPH, N.A. 1.45, Olympus), a filter set (GFP-4050B, Semrock), mercury lamp (U-HGLGPS, Olympus), a CMOS camera (DMK33UX174, Imaging Source), and an optical table (HAX-0806, JVI). Projection of the image to the camera was made at 0.058 μm per pixel. Sequential images were acquired by the imaging software (Solis, Andor) as 16-bit images under 25-ms intervals.

Negative stain TEM

For measuring flagellar filament lengths, overnight cultures were gently washed from MHT plates into PBS and washed 1x with PBS, followed by fixation with 1% EM grade glutaraldehyde in PBS on ice for 10 minutes. Fixed cell suspensions were centrifuged and resuspended in water and kept on ice. Samples were applied to glow-discharged carbon-coated copper grids (Agar Sciences) and stained with 2% uranyl acetate. Images were collected on a FEI T12 TEM at an acceleration voltage of 120 kV at a nominal magnification of 6,500x. Filament lengths were measured by hand in FIJI.

Electron cryotomography and subtomogram averaging

Strains to be imaged for subtomogram averaging were washed off plates and concentrated to an O.D.₆₀₀ of 10-20 and mixed with 10 nm gold fiducial markers (Sigma-Aldrich) in 5% BSA. Samples were applied to Quantifoil R2/2 grids and plunge frozen in liquid ethane using a Vitrobot (FEI). Imaging was performed on a Thermo-Fisher Glacios 200 kV electron microscope equipped with a Falcon 4 direct electron detector and Selectris energy filter.

Tomograms were reconstructed using a combination of IMOD 4.11.8 for fiducial modeling and Tomo3D for SIRT tomographic reconstruction.^{61,62} To enhance the contrast of tomograms for display of unaveraged motors and to measure disk diameters, tomograms were CTF-deconvolved as first described by (Tegunov and Cramer 2019)⁶³ but with CTF deconvolution performed in 2-D on the tilt series prior to 3-D tomographic reconstruction. In short, the procedure restores the magnitude of the low-resolution components that are attenuated by the CTF while removing the noisy components at medium and high resolution, which results in an overall contrast improvement. This code is available in version 2.2 of Tomo3D.

For subtomogram averaging, particles were picked using 3dmod from the IMOD suite and imported into Dynamo 1.1.532 for subtomogram averaging. We imposed C17 symmetry for averaging based upon established prominent symmetry of the periplasmic structures of the *C. jejuni* motor.

Subtomogram averages of motors in this work have been deposited with the Electron Microscopy Data Bank (EMDB) under the following accession numbers: EJC168 12.5 ng/mL ATc: EMD-17769; EJC168 25 ng/mL ATc: EMD-17770; EJC168 50 ng/mL ATc: EMD-17771; EJC168 100ng/mL ATc: EMD-17772; *flgP*^{AAA}: EMD-17773; *flgP*^{Δ18-62}: EMD-17774; *flgP-lpp*⁵⁵: EMD-18274; *ΔflgPQ*: EMD-17775; *ΔflgPQ Δ0661 ΔkpsD ΔpglAB::aphA*: 17776.

Chicken colonization assays

Chick colonization assays. The ability of WT *C. jejuni* 81–176 *rpsL*^{K88R} and isogenic mutants to colonize chicks after oral inoculation was determined as previously described (32). Briefly, fertilized chicken eggs (SPAFAS) were incubated for 21 days at 37.5 °C with appropriate humidity and rotation in a Digital Sportsman model 1502 incubator (Georgia Quail Farms Manufacturing Company). One day after hatch, chicks were orally inoculated with 100 μ L of phosphate buffered saline (PBS) containing approximately 180–240 CFU WT or mutant strains. Strains were prepared for infection after 16 h growth at 37 °C under microaerobic conditions on MH agar by suspending *C. jejuni* strains in MH broth. Dilution series in PBS were performed to achieve the appropriate inoculum for oral gavage of chicks. Dilutions of the inoculum were plated on MH agar to assess the number of bacteria in each inoculum. At 7 days post-infection, chicks were sacrificed, the cecal contents were removed and suspended in PBS, and serial dilutions were plated on MH agar containing trimethoprim and cefoperazone. Following 72 h of growth at 37 °C in microaerobic conditions, bacteria were counted to determine CFU per gram of organ content. Recovered colonies were analyzed by colony PCR to verify that WT and mutant strains were isolated from respectively infected chicks.

Whole genome sequencing

Whole genome sequencing was performed by Source Biosciences (U.K.). Genomes were assembled and analysed using the software package Geneious Prime 2021.0.3 (Biomatters, New Zealand). The paired reads provided by Source Biosciences were imported into Geneious and trimmed using BBDuk, removing adapters and low-quality reads. Whole genome sequencing reads of parental strains *flgP-lpp*⁵⁶ and Δ *flgPQ* were mapped to a *C. jejuni* reference genome NC_008787. These assembled genomes were then used as reference genomes against which suppressor genomes were assembled and analysed. We used the Geneious variant finder to find mutations in each sequenced suppressor genome relative to its parental reference genome, characterise mutation frequency and its possible effect on codon and amino acid changes.

Phylogenetics

A phylogenetic tree of the *Cjj_81176_0661* family was determined using the sequences allocated to the PFAM PF04748 family as downloaded on 17th May 2022 and performing a multiple sequence alignment using RAxML with a Jones-Taylor-Thornton (JTT) model of amino acid substitution rates with a discrete gamma distribution.

QUANTIFICATION AND STATISTICAL ANALYSIS

Quantification and statistical analyses were carried out using GraphPad Prism (v10.1.1). For comparison of two groups, e.g. comparing swimming speed of two mutants, a two-tailed t-test was performed and difference were considered significant if $p < 0.05$. For comparisons of >2 groups, 1- or 2-way ANOVA was used for statistical analysis. Number of replicates, p-values and SEM are provided in figures and figure legends.